Preprint Cambridge Centre for Computational Chemical Engineering ISSN 1473 – 4273

Multivariate characterisation of lactose powder and granules of a wet granulation process

Jan-Georg Rosenboom[1], Sergiy Antonyuk[2], Stefan Heinrich[2], Markus Kraft[1]

released: 30 July 2013

[1] Department of Chemical Engineering and Biotechnology
University of Cambridge
New Museums Site
Pembroke Street
Cambridge, CB2 3RA
United Kingdom
E-mail: mk306@cam.ac.uk

[2] Institute of Solids Process Engineering and Particle Technology
Hamburg University of Technology
Denickestraße 15
21073 Hamburg
Germany
E-mail: antonyuk@tuhh.de

Preprint No. 132

Keywords: wet granulation, multivariate characterisation, lactose powder, granules

Edited by
Computational Modelling Group
Department of Chemical Engineering and Biotechnology
University of Cambridge
New Museums Site
Pembroke Street
Cambridge CB2 3RA
United Kingdom

Fax: + 44 (0)1223 334796
E-Mail: c4e@cam.ac.uk
World Wide Web: http://como.cheng.cam.ac.uk/

Abstract

In this work, α-lactose monohydrate powder and the granules produced from this powder by a high-shear granulation process are characterized with respect to size, shape, porosity and strength using various analytical methods. The multivariate data set includes an assessment of the applicability and reproducibility of each measurement technique. Particle size distributions are obtained by static image analysis (SIA), laser scattering (LS) analysis and sieving. Granule porosities are determined using individually developed procedures for X-ray computed tomography (μCT) and mercury intrusion porosimetry (MIP). Lactose granules show absolute porosities increasing from 30% to 40% along the size classes. Filling pressure adjustment for granules smaller than 600 is required to overcome the limit for interstitial void intrusion at the standard mercury filling pressure of 1 psia. The μCT derived visual information of larger granules shows internal pore structures with denser cores and porous shell parts. Particle surface roughness is approached using atomic force microscopy (AFM), scanning electron microscopy (SEM) and μCT. A reasonable range to estimate heights of asperities on lactose powder particles may feature values up to about 800 nm. The strength of the product granules is measured via uniaxial compression testing. The compression strength of the granules, derived from the largest failure peaks at low displacement, follows a logarithmic decrease with size from 1.2 to 0.2 MPa.

Contents

Abbreviations

AFM	Atomic force microscopy
BET	Brunauer-Emmett-Teller gas adsorption
COV	Coefficient of variance
DI	De-ionized
HF	Hole-filled or hole-filling
HFE	Hole-filling error factor
LS	Laser scattering
μCT	X-ray computed tomography for small objects
MF	Magnification factor
MIP	Mercury intrusion porosimetry
PSD	Particle size distribution
RI	Refractive index
SEM	Scanning electron microscopy
SIA	Static image analysis
SSE	Sum of squared errors
TH	Threshold
XRD	X-ray diffraction

1 Introduction

The properties of pharmaceutical tablets such as strength and dissolution behaviour are key factors of their quality [1]. Subsequently, in order to derive high quality tablets, the excipient material, which affects such properties, needs to be of high quality, as well [2, 3]. Most commonly, this material is an agglomerated version of a digestible powder, e.g. lactose, derived from a high-shear wet granulation process [2]. Important properties of the resulting granules are size, porosity, strength, flow properties and dissolution behaviour [2, 4]. The success and efficiency of the production of granulated materials with desired properties depend to a large extent on 1) how well the granulation process and the influencing process parameters are understood and 2) how well these phenomena are implemented in computer models to predict the process output and to design the industrial machinery necessary to conduct the process [2, 5]. The prediction of the experimental output based on given process parameters by a computer model is a desired ability. The kinetics and interaction of forces upon particles during granulation, however, are still poorly understood. In order to gain better understanding of granulation processes and develop models further from an investigation-oriented level towards industrially applicable tools, we require highly detailed and rigorously characterising data sets for granulation materials of industrial interest [6].

Among others, Takano et al. (2002), Narayan and Hancock (2003), Adi et al. (2007), Mangwandi et al. (2010) and Wikberg and Alderborn (1991) investigated lactose powders and the granules from different granulation processes with respect to varying properties such as size, strength, porosity and surface structure [1, 7–10]. Rahmanian et al. (2011) used calcium carbonate powder and polyethylenglycol binder in another high-shear granulator [11]. Mechanical strength of different granules was investigated by several authors [9, 11–15]. Cheong et al. (2005) characterised the critical displacement and fracture point by a rapid reduction in the compressive force during compression testing and a visible meridian crack splitting the granule in two halves [13]. A survey through the literature on lactose granulation shows that numerous studies have been undertaken to characterise lactose granulation materials and the influencing process parameters. The formulations of the initial material and the granulation setup vary. Further, detailed quantitative information and challenges associated with the measurement techniques are rarely reported [7, 9–11, 13]. The combination of process parameters, materials and equipment as well as the interaction of these influencing factors lead to a complexity that 1) makes comparability of experimental granulation results difficult, 2) necessitates carefully analysed and critically reviewed data and 3) makes process predictions by simulations challenging, which again necessitates high-quality data for model evaluation and understanding of the matter.

The purpose of this paper is to present a detailed and multivariate characterisation of α-lactos monohydrate and the granules produced from this powder by an exemplary high-shear granulation process. The properties characterised include size, shape, porosity, surface structure and strength. The granule properties were determined per sieve cut (19 sieve classes were obtained after size classification) in order to increase the data resolution for comparison with discrete computer model outputs and to understand dependencies on size

in general. The data set is intended to be used as a data basis for computer models such as the multidimensional population balance based approach by Braumann et al. [5, 16–19]. Particle properties were assessed with multiple techniques. The multivariate data set includes an assessment of the applicability and reproducibility of each measurement technique. Particle size distributions were obtained by static image analysis (SIA), laser scattering (LS) analysis and sieving. Granule porosities were determined using individually developed procedures for X-ray computed tomography (μCT) and mercury intrusion porosimetry (MIP). Particle surface and roughness characterisation was approached using atomic force microscopy (AFM), scanning electron microscopy (SEM) and μCT. The strength of the granules was measured via uniaxial compression testing.

In section 2, the granulation setup for the production of lactose granules is explained. In section 3, all analysis methods for the characterisation of the granulation materials are described. Section 4 discusses the analytical results with respect to the properties mentioned above for 1) the initial lactose powder and 2) the granulated material.

2 Wet granulation setup

In the following we study a high-shear wet granulation of Granulac 230 α-lactose monohydrate powder from Meggle, Germany, with de-ionised water as the binder. The experimental setup used in this work was established during the course of earlier studies and is presented schematically in **Figure 1** [20].

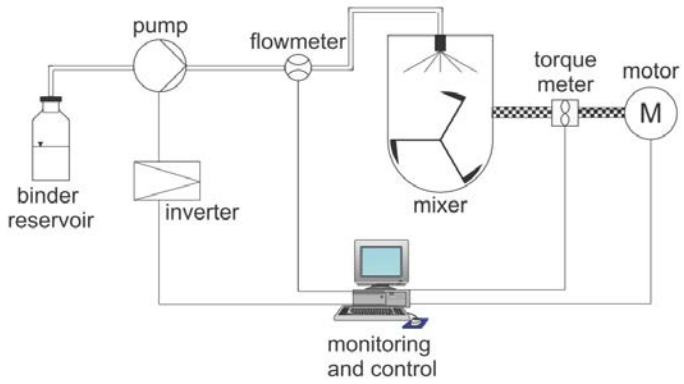

Figure 1: *Experimental granulation setup. Image taken from [20].*

A horizontal axis ploughshare mixer described by Jones and Bridgwater (1997) was used in this work [21]. The mixer-granulator consists of a 5 L mixing chamber and a motor-driven horizontal shaft that turns six V-shaped ploughs, each offset by 120° or 180°, plus 2 scraping blades at either shaft ends. The mixer chamber is 22.5 cm long, the bowl radius (approximately equal to each plough's length) is 7.5 cm and the headboard height above the main shaft is 15 cm. 1 cm above that is the outlet of a single fluid spray nozzle (model 121, d = 0.5 mm, 60° spray angle, Düsen-Schlick, Germany) including drip cup, all mounted to a transparent plastic box on the granulator. The nozzle is fed with the

binding liquid (de-ionised water) from a peristaltic pump (model DBP 764, Dylade Fresenius, UK). The binder is drawn from a reservoir by a magnetic drive gear pump (model DG.19, Tuthill Corporation, USA). The pump speed is set by an inverter (model Altivar 31, Telemecanique, France) and recorded by a flow meter (OG1, Nixon Flowmeters, UK), both of which are connected to a computer via two data recording cards (6009 and 6601, National Instruments, USA). A labview program monitors the pulses from the flow meter and sends signals to the inverter to control binder flow. Similarly, the mixer speed is controlled and monitored via signals to the built-in DC mixer-motor (Kemutec, USA) and speed pulses from the torque meter (DRBK-20-n, ETH Messtechnik, Germany), respectively. The timing of the process steps (agitation, binder addition, post-binder mixing) is facilitated by the labview program as well. Granulac 230 α-lactose monohydrate as the granulation material was purchased from Meggle, Germany. After granulation, the granulation product was collected from the granulator with brushes. The material was spread over aluminium trays and dried in an oven at 60°C before sieving. The process parameters are given in table 1 and were set according to preliminary studies [20].

Table 1: *Granulation process parameters*

Process Parameter	Value
Amount of lactose powder	1 kg
Amount of binder (DI water)	150 ml
Mixer speed	120 rpm
Time for pre-mixing	2 min
Time for binder addition	2 min
Time for post-binder addition mixing	5 min

3 Experimental analysis methods

In the following, the analysis techniques used for lactose particle and granule characterisation are described. Table 2 gives a brief overview. In this work particle size distributions are presented as fraction frequencies of the form:

$$w_{0,i} = \frac{n_i}{n_{\text{total}}} \text{ or } w_{3,i} = \frac{V_i}{V_{\text{total}}}, \tag{1}$$

where $w_{0,i}$ is the number fraction of particles in size class i, n_i is the number of particles in size class i and n_{total} is the total number of particles in the observed population. $w_{3,i}$ describes the volume fraction with V_i being the volume of particles in size class i and V_{total} being the total volume of particles in the observed population, accordingly.

Table 2: *Characterisation techniques used in this work*

Measured properties	Analysis methods
Lactose powder particles	
Particle size distributions (PSD)	Static image analysis (SIA)
	Laser scattering (LS)
Surface topography	Static image analysis (SIA)
	Atomic force microscopy (AFM)
Porosity, crystallinity	BET surface analysis
	X-ray diffraction (XRD)
Lactose product granules	
Particle size distributions (PSD)	Sieving
Surface topography, shape	Scanning electron microscopy (SEM)
Porosity	Mercury intrusion porosimetry (MIP)
	X-ray computed tomography (μCT)
	Compression tests

Sieving of 75 g split samples of dried granulation product granules was performed in 3 tiers of 6 Endecotts sieves with apertures along the sieve stack following a $\sqrt{2}$ progression from 53 μm up to 16000 μm for 20 minutes [20].

Static Image Analysis (SIA) of lactose powder was performed using a Malvern Morphologi G3s to derive number based particle size distributions (PSD) and convexity of the powder particles. Convexity is expressed as the ratio of the convex hull perimeter and the actual perimeter. It takes values up to 1 with lower values indicating higher surface roughness. This measure is independent of the form of the particle and therefore was used for the estimation of the height of asperities on primary particle surfaces. The appropriate sample volume for dispersion was chosen to be 5 - 7 mm^3 as those were found to result in sufficient dispersion after air injection. Measurements of very large subsamples did not deliver more information than sub-samples including 30000 to 60000 particle datapoints. 20$\times$ optical magnification, at least 2 bar dispersion pressure and the application of intensity filters were found to be appropriate settings for SIA analysis for particles of all sizes.

For **Laser Scattering (LS)** analysis of lactose powder a Beckman Coulter LS230 was used to derive volume based PSD in the range of approximately 0.3 μm to 2000 μm under the assumption of spherical particles [2, 4]. Lactose powder samples were subjected to 2% - 4% suspensions by weight in hexane and ethanol. Ethanol has previously been used as the suspending medium and is relatively inexpensive compared to hexane [8]. Hexane was initially chosen to be the suspending medium because it was available and shows lower solubility of lactose and better wettability [22]. Sample suspensions were gently stirred in the beaker in order to avoid extensive breakage of agglomerates. Some sample suspensions were sonicated in an ultra-sonic bath for 6 minutes to study the influence of sonication on the breakage of agglomerates. The initial material for granulation does not

undergo sonication prior to granulation and is therefore more likely to be agglomerated. Each sample was measured in three subsamples as in other studies [1, 8, 9]. The refractive index used for lactose was 1.533 with an imaginary part of 0.1 for white powders to account for absorption [8, 23]. The refractive index used for laboratory reagent-grade hexane fraction (Fisher Scientific) was determined in an ABBE60 refractometer to be 1.378. The refractive index used for ethanol was 1.361 [8].

Atomic Force Microscopy (AFM) was performed using a Veeco Dimension 3100 in concert with SEM and SIA measurements. A range of reasonable values for lactose particle asperity heights, h_a, was established for use in granulation models as those commonly use h_a in Stokes criterion calculations to determine whether particle collisions lead to coalescence [4, 5]. Primary lactose particles were immobilized with candle wax on silicon wafers. A tapping-mode cantilever tip was used. A tracing frequency of 0.2 Hz was used in the experiments.

Scanning Electron Microscopy (SEM) was used for high-resolution surface and shape analysis. Lactose powder was imaged using a Phenom G2 desktop SEM which allowed for direct measuring of length scales, e.g. surface asperities, in the SEM pictures. Lactose granules were measured with a JEOL JSM-820 electron microscope. The voltage was set to 5 kV to avoid charging of the sample.

Surface area and porosity (BET) analysis of lactose powder via nitrogen gas adsorption at liquid nitrogen temperature (77.35 K) was performed using Micromeritics TriStar 3000 V6.08 A and ASAP 2020 V3.04 H surface area analysers. The incentive behind measuring lactose, which is usually produced by crystallization from supersaturated solutions and milled to desired sizes, was to investigate whether the initial particles can be readily assumed as purely dense solids in computer models [5, 20, 24–27]. 2 g of powder were used, resulting in BET correlation factors above 0.999, usually indicating applicability of the method. In order to remove contaminants and residual moisture prior to porosity measurements while conserving chemical stability of the samples, vacuum drying at 70°C overnight was applied for degassing lactose powder and granule samples.

X-ray computed tomography (μCT) was used as a non-invasive and visual technique to characterise porosity of granules. The X-ray tomograph used in this study was a Skyscan 1072 with a maximum pixel resolution of 4 μm. Lactose granules of appropriate size classes (i.e., greater than 100 μm and smaller than 13200 μm) were immobilised by packing in a straw or wrapped plastic foil which was fixed to the rotating stub inside the X-ray tomograph with sticky dough. Due to the limited space and field of view of the X-ray camera, sample size, i.e. number of granules, decreases with increasing particle size. 55 kV voltage, 3.4 s exposure time and angle increments of 0.45° were used. The procedure to evaluate each horizontal slice image of the granule ensemble along the height using ImageJ is explained in **Figure 2** and can be described in brief as:

1. Binarise raw stack slice images with threshold (TH);
2. Measure overall dark pixel fraction A_{TH};
3. Use 'hole-filling' option on raw stack slice images with threshold;

4. Measure overall dark pixel fraction A_{HF} ;

5. Calculate void fraction via Equation 2.

$$\text{Void fraction} = \mathrm{VF} = \frac{\text{void area}}{\text{hole-filled area}} = \frac{A_{\mathrm{HF}} - A_{\mathrm{TH}}}{A_{\mathrm{HF}}}. \tag{2}$$

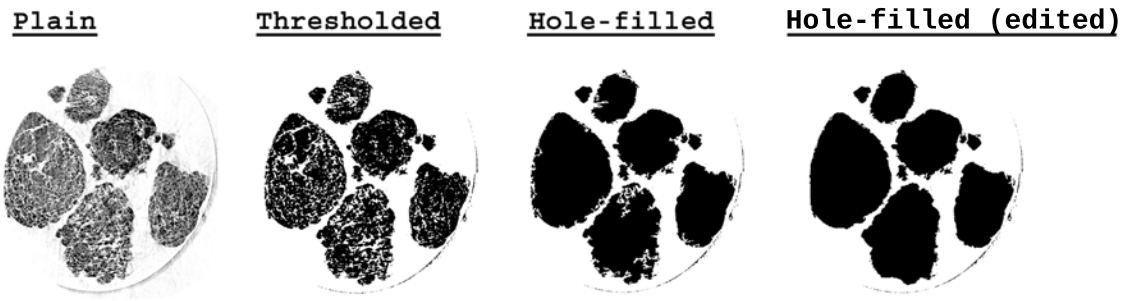

Figure 2: *X-ray tomography (μCT) analysis procedure for the example of $\leq$2360 μm granules. The postprocessing included binarising all raw images to derive the porous granule pixel area, hole-filling in ImageJ to derive the granule envelope area. The difference in black pixel area gave the void fraction as porosity for each image slice. Additional hole-fill editing was performed on single images with PhotoShop to assess the associated error for the whole stack.*

By averaging the results along the vertical direction we derive averaged void fractions per size class that can be interpreted as particle porosity. In order to infer from the average porosity of the sample to that of the whole population in a size class we assume that 1) all particles in a size class have the same porosity and 2) every single granule is uniformly porous. Both assumptions were visually found to be valid for most particles while some specimen presented clear exceptions. For example, in **Figure 3** the ensemble of $\leq$425 μm granules (left image) shows some particles that look slightly denser than others. The right image in Figure 3 displays a slice image through one single $\leq$4750 μm granule which visually exhibits a denser core and a more porous shell part. This method also provides a porosity profile along the granule height if one single granule is measured (see supplementary material section).

Hole-filling is sometimes incomplete as visible in Figure 2 and the systematic error was assessed by manual editing of some binarised images. Single thresholded slice images were evaluated according to the aforementioned protocol and with additional manual hole-filling with Adobe Photoshop. The ratio of that to the formerly derived value for each size class was recorded as a hole-filling error factor (HFE), which showed a logarithmic increase towards smaller sizes. The values are given in the results section. The resolution of 1024 $\times$ 1024 pixel per X-ray image in combination with the applied magnifications (from 20$\times$ to 70$\times$) limit the detectability of pore to about 4 μm. Smaller pores fall below the minimum pixel resolution and thresholding may cause additional loss of information. Thus, the results from μCT can generally be considered as as 'large-scale'

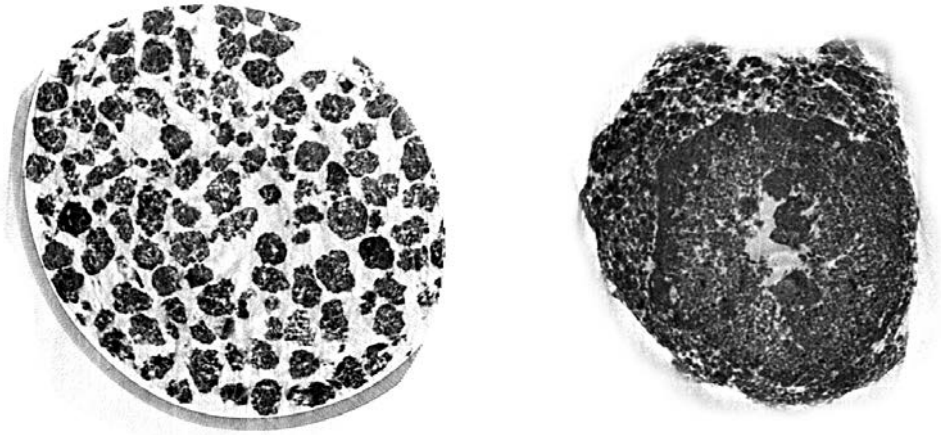

Figure 3: *X-ray tomography (μCT) example images of an ensemble of $\leq$425 μm granules and one large $\leq$4750 μm granule.*

(≥ 4 μm) porosity. A magnification factor (MF) as the ratio between 50$\times$ as the reference and the applied magnification is in place to correct for the influence of magnification on detectability of small pores. The final and adjusted porosity $P_{\mu\mathrm{CT}}$ derived from μCT can then be calculated via the void fraction VF from ImageJ scaled by HFE and MF:

$$P_{\mu\mathrm{CT}} = \mathrm{VF} \cdot \mathrm{HFE} \cdot \mathrm{MF} = \frac{A_{\mathrm{HF}} - A_{\mathrm{TH}}}{A_{\mathrm{HF}}} \cdot \frac{\mathrm{VF\ (edited\ hole\text{-}filling)}}{\mathrm{VF\ (automated\ hole\text{-}filling)}} \cdot \frac{50}{\mathrm{Magnification}}. \quad (3)$$

Mercury intrusion porosimetry (MIP) was used to quantify lactose granule porosity P alongside the visual information and ' large-scale' data from X-ray tomography.

$$P = (1 - \frac{\rho_{\mathrm{e}}}{\rho_{\mathrm{s}}}) = (1 - \frac{V_{\mathrm{s}}}{V_{\mathrm{e}}}), \quad (4)$$

where P is the overall porosity, ρ_e and ρ_s are the envelope and skeletal densities, respectively, and V_e and V_s are the envelope and skeletal volumes of a granule, respectively. Skeletal density is measured at highest mercury intrusion pressure and the envelope density at appropriate low intrusion pressures. Based on results from X-ray tomography images, the granules were assumed to have closed pores which will collapse under pressure and thus give a bias to a pore size calculation. Therefore, pore size distribution was not considered in this work. Absolute porosity is not affected by collapsing pores [28, 29]. The Washburn equation was used to calculate appropriate mercury filling pressures at which the solid samples' envelope density is measured:

$$d_{\mathrm{P}} = \frac{-4\gamma\cos\theta}{P_{\mathrm{abs}}}, \quad (5)$$

where d_{P} is the pore diameter, γ is the surface tension usually taken at 0.485 N/m, θ is the wetting angle of mercury on most surfaces taken to be 130° and P_{abs} is the applied

mercury intrusion pressure [28, 30]. Smaller granules need to be measured using higher filling pressures as their interstitial spaces are smaller. If insufficient pressure is applied, all unfilled interstitial space will falsely be counted as porosity. In order to use Eq. (5) to calculate appropriate filling pressures, the gap size between particles was approximated by the geometric calculations of circular pores between 4 adjacent spheres, resulting in $d_{\text{gap}} = 0.414\ d_{\text{particle}}$. **Table 3** shows that for the size classes below 425-600 μm a higher filling pressure than the machine standard of 1.02 psi was required for unbiased porosity calculation.

Table 3: *Adjusted filling pressures for mercury intrusion porosimetry of smaller granules and their associated interstitial spaces (d_{gap}).*

d_{particle} [μm]	d_{gap} [μm]	P_{fill} [psi]
56-75	23	**7.80**
75-106	31	**5.82**
106-150	44	**4.12**
150-212	62	**2.91**
212-300	88	**2.06**
300-425	124	**1.46**
425-600	176	**1.03**
600-850	249	0.73
850-1180	352	0.51

Samples from each size class were dried at 70°C under vacuum over night prior to insertion into a Micromeritics AutoPore IV 9500 V1.06 porosimeter. The penetrometer volume was 5.6 ml and the stem volume was 0.4 ml. Sample sizes of 0.2 g - 0.3 g were used to prevent exceeding of stem volume capacity. The weight of the empty and calibrated penetrometer and the solid sample were measured with a weight scale (Mettler-Toledo AG204) that was accurate to 0.0002 g. Every sieve cut was measured once and three size classes were measured twice to assess the reproducibility of the measurements. The resulting standard deviations were all below 1% of the average. The error associated with mercury intrusion was previously estimated to be less than 2% [31]. For larger sizes, only 10 or less specimen could be measured, due to limited space in the penetrometer and requirements for sample size as outlined in Section 3. The trade-off between measurable granule size and sample size was similar as for μCT. 95%-confidence intervals were computed similarly using a normal error distribution for large numbers of specimen and the t-statistic was used for small specimen numbers, respectively. The confidence intervals in each size class were calculated based on the maximum observed standard deviation (1%) and the estimated number of specimen in each measurement.

For **single granule strength testing**, granules from 10 different granulation product sieve cuts were compressed in an Instron 5567. The compression velocities were chosen to be 0.5 mm/min for sizes $\leq 850\ \mu$m and 2 mm/min for sizes $\geq 850\ \mu$m. Between these velocities, compression strength results were reproducible within the range of 5% uncertainty. 10 specimen were tested for every sieve class and sample runs with high variation (larger

than 50% of the average) were repeated. As in [9, 11–14], the critical tensile strength formula by Hiramatsu and Oka was used:

$$\sigma_t = 0.7 \cdot \frac{F_0}{\pi(d/2)^2}, \tag{6}$$

where F_0 is the critical load at failure, d is the diameter of the granule derived by size classification, e.g. sieving. The main challenges of this strength testing analysis are the deformability and fragmentation of lactose granules. In contrast to metallic or ceramic materials which mostly produce one distinct stress peak at fracture followed by a significant drop in stress, the agglomerates showed more than a single peak and partial fracture of granule surface parts could be observed. During μCT analysis we observed that at least for larger granules the outer shell of a granule is sometimes more porous than the denser core part, which potentially leads to plastic deformation and partial fracture before the major part of the granule breaks (see Figures 3 and 11). The compression strength in this study was derived from the maximum peak followed by a clear drop in compression stress in the smaller strain region ($\varepsilon \leq 0.3$) as suggested by [13], where distinct meridian cracks of larger granules could be visually observed, assuming that this peak appropriatly represents the strength of the whole granule.

4 Analytical results and discussion

4.1 Initial powder characterisation

4.1.1 Particle size and shape distribution

The SIA derived mean diameters are $d_{n,\text{mean}}$ = 6.67 μm (arithmetic number average) and $d_{v,\text{mean}}$ = 41.65 μm (arithmetic volume-based average). The breadth of the distribution is described by a span$_n$ = 2.75 and span$_v$ = 1.47. The span is defined via quantiles as (d_{90} - d_{10})/d_{50}. LS measurements with Granulac 230 lactose powder derived $d_{v,\text{mean}}$ = 27 - 30 μm, depending on the sample preparation, and a slight bimodality. The major peak of the PSD around the mean is accompanied by a comparatively small but significant mode of finer material. The fines peak disappears when the imaginary part of the refractive index is set from the literature value 0.1 to 0. The breadth of the distribution is characterised by a span$_v$ = 2.1. **Figure 4** compares results from LS using sonication with non-sonicated samples. The respective characteristic distribution shape parameters are presented in the supporting materials section. The additional lines are 95% confidence bands. The variance in the results is higher for non-sonicated samples than for samples with sonication. The results are contrary to findings by Adi et al. (2007), who reported a clear decrease in size and modality for micronised lactose in propanol suspension sonicated for 5-10 minutes [8]. The independence of lactose PSD on sonication in this work indicates that the sample treatment by syphoning and pipetting causes enough breakage of the agglomerates to outbalance the sonication effect and that breakage due to sample preparation cannot be

avoided.

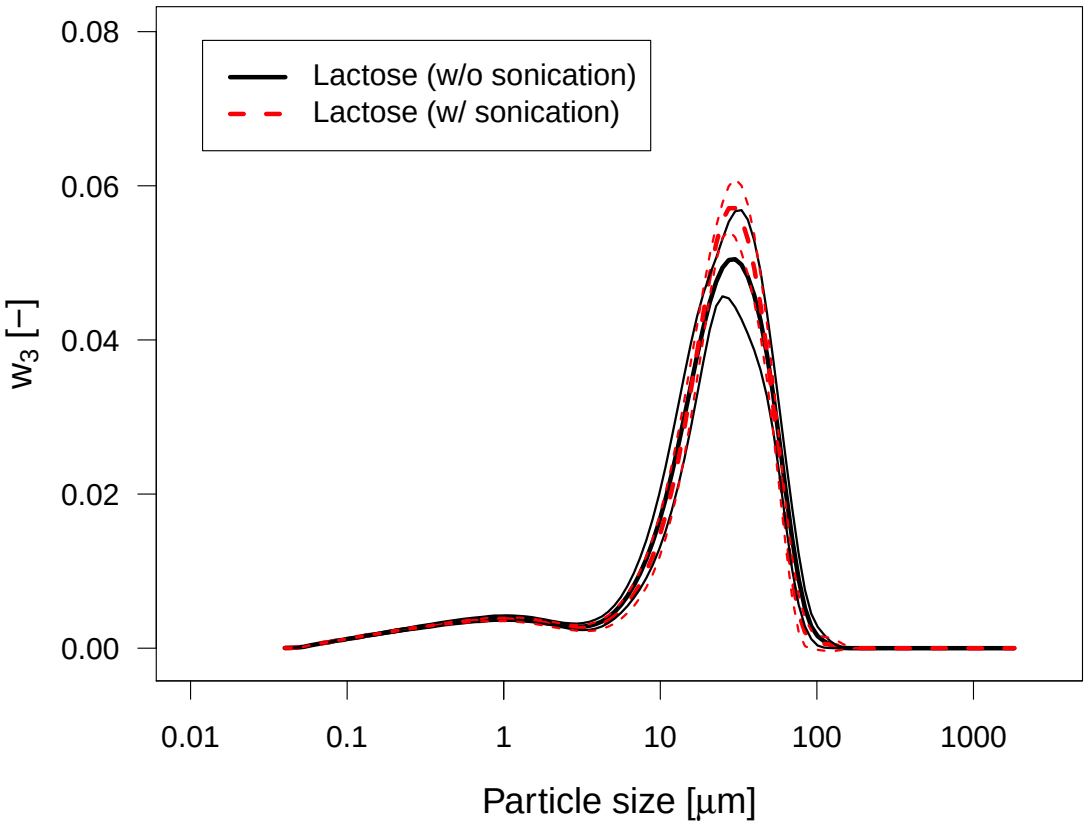

Figure 4: *Volume based PSD for lactose monohydrate powder derived from laser scattering including and excluding prior sonication for 6 minutes.*

PSD obtained with ethanol show less distinction between fines and coarse modes than those obtained with hexane (see plots in supporting material). A reason for this disparity could be the improved wettability of hexane compared to ethanol and the resulting agglomerate breakage and particle separation [22].

For comparison, Mangwandi et al. (2010) reported bimodality and a PSD derived from LS with a median $d_{v,50}$ = 33 μm for the same material, which is higher than $d_{v,50}$ = 25 observed in this work [9]. Chitu et al. (2011) reported a span$_v$ = 2.3 for an α-lactose monohydrate from Fisher Scientific with a higher $d_{v,\text{mean}}$ of 60 μm.

4.1.2 Lognormal fitting to PSD

Population balance granulation models often generate the initial powder via a monomodal number-based lognormal distribution which is described by the two lognormal parameters $\mu_{\log}$ and $\sigma_{\log}$. Those can be estimated via experimental data fitting. If the initial model distribution is to be sampled as particle volumes, which is reasonable regarding the purpose of a computer model to compare the output with volume based experimental data,

w_3 results for lactose powder from LS can be used for lognormal fitting. Monomodal and bimodal distributions (as a combination of two weighted lognormal distributions), were fitted to SIA and LS particle size distributions using the least-squares optimisation routine *optim()* in the statistical software environment R. For monomodal distributions the routine was set up to minimise the squared residuals of the model and the measured PSD by optimising $\mu_{\log}$ and $\sigma_{\log}$. For the bimodal distribution of the form $\tau \times f(\mu_{\log,1}, \sigma_{\log,1}) + (1 - \tau) \times f(\mu_{\log,2}, \sigma_{\log,2})$ the two additional $\mu_{\log}$ and $\sigma_{\log}$ for the second mode and a weighting factor τ between 0 and 1 were optimised. Lognormal distributions fitted to LS data are presented in **Figure 5**. A summary of the characteristic lognormal location and shape parameters derived for the experimental w_0 and w_3 PSDs are presented in **Table 4**. In computer models, often the exponentials of lognormal parameters are used.

Table 4: *Lognormal distribution parameters for monomodal and bimodal distributions fitted to w_0 and w_3 PSD data. τ is the weighting factor for the bimodal distribution. s means sonicated LS sample, n/s means non-sonicated.*

	$\mu_{\log,1}$ [-]	$\sigma_{\log,1}$ [-]	$\mu_{\log,2}$ [-]	$\sigma_{\log,2}$ [-]	τ [-]
SIA w_0 monomodal fit	1.50	0.89	-	-	-
LS w_3 (s) monomodal fit	3.10	0.84	-	-	-
LS w_3 (n/s) monomodal fit	3.07	0.91	-	-	-
LS w_3 (n/s) bimodal fit	0.45	1.60	3.33	0.59	0.18

4.1.3 Surface roughness investigation

Figure 6 shows SEM images of Granulac 230 α-lactose monohydrate particles. Most particles look non-spherical and edgy with generally smooth surfaces that exhibit distinct asperities and some fine slices or cracks. The typical look of lactose crystals was described in the literature as tomahawk- or wedge-shaped [32, 33]. Since lactose is classified as a cohesive powder, most of the surfaces' unevennesses are likely to be small particles adhering to the surfaces of coarser ones, which was reported by several authors [8, 34]. Those may be interpreted as asperities as they influence the contact surface for major particle collision during granulation. The Phenom SEM software allowed for measurement of length scales on 2D images. The evaluation of randomly chosen particles and their asperities resulted in roughness values ranging from 0.1 - 1.8 μm, with larger particles having larger measurable asperities.

As another method of roughness quantifiction, AFM was used where successful, i.e. where good tip retracing was achieved, to record the characteristic roughness values $R_{\max}$, R_z (average over 5 highest peaks and 5 lowest valleys), R_a (arithmetic average), R_q (geometric average). **Figure 7** shows an example of 3D surface topographies derived from different surface areas on the poured lactose sample. The maximum peaks measured with AFM, which are mostly significantly higher than the measured average, somewhat agree with the SEM evaluations of single distinct asperities on selected particles. However, it

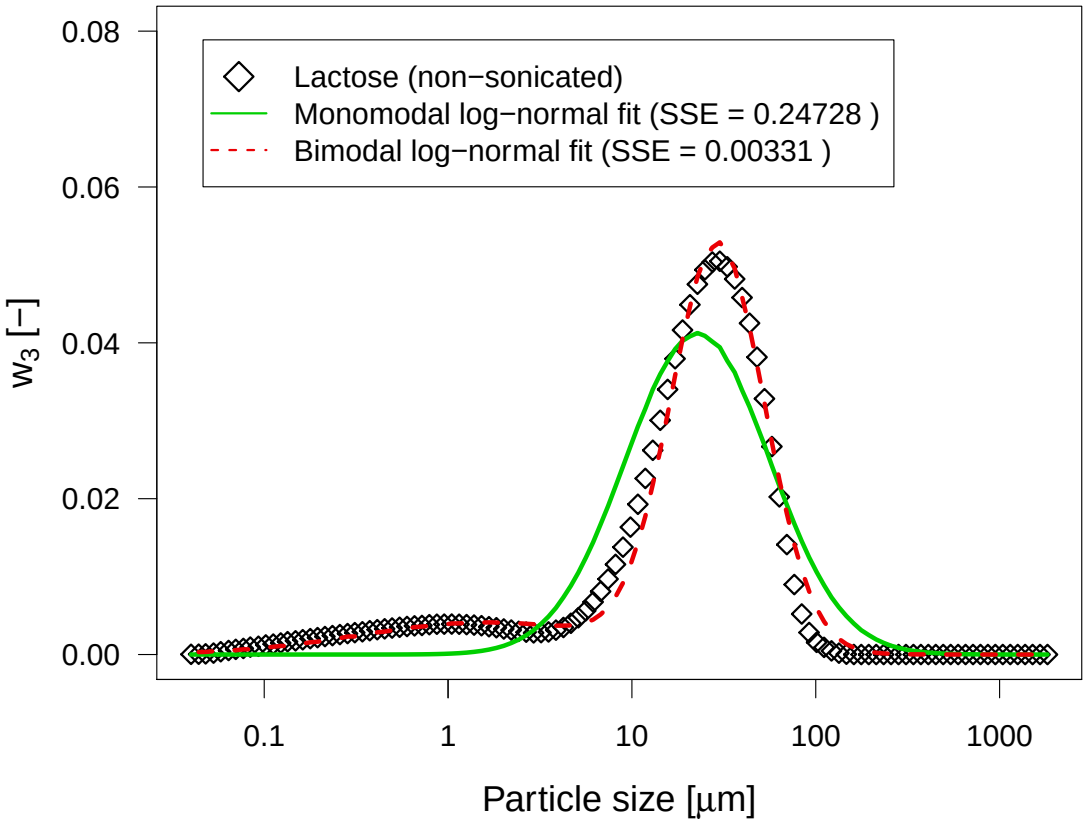

Figure 5: *Monomodal and bimodal lognormal distributions fitted to volume based PSD for lactose monohydrate from laser scattering. SSE is the sum of squared errors.*

may be more useful to use the average roughness values to establish a range for asperity height for the assessment of roughness [35]. Depending on which of the averages is chosen, average height of asperities range up to 0.7 μm. The established range of asperity heights may be used for the choice of appropriate values for h_a in computer models such as the one from Braumann et al. (2007) [5].

SIA derived particle convexity can be used for asperity estimation. With the assumption of circular particle shape and assuming that the convexity as described in Section 3 is reasonably proportional to a ratio of a fictional smooth particle perimeter to the perimeter around the particle's asperity heights, one can estimate the height of asperities via

$$\text{convexity}\,\omega \approx \frac{\text{smooth circle perimeter}}{\text{(smooth circle + roughness) perimeter}} = \frac{\pi x}{\pi(x+2h_a)} \tag{7}$$

$$\Longrightarrow h_a = \frac{x}{2}\cdot\left(\frac{1}{\text{convexity}} - 1\right). \tag{8}$$

The estimation of height of asperities by this method is admittedly rough, due to the

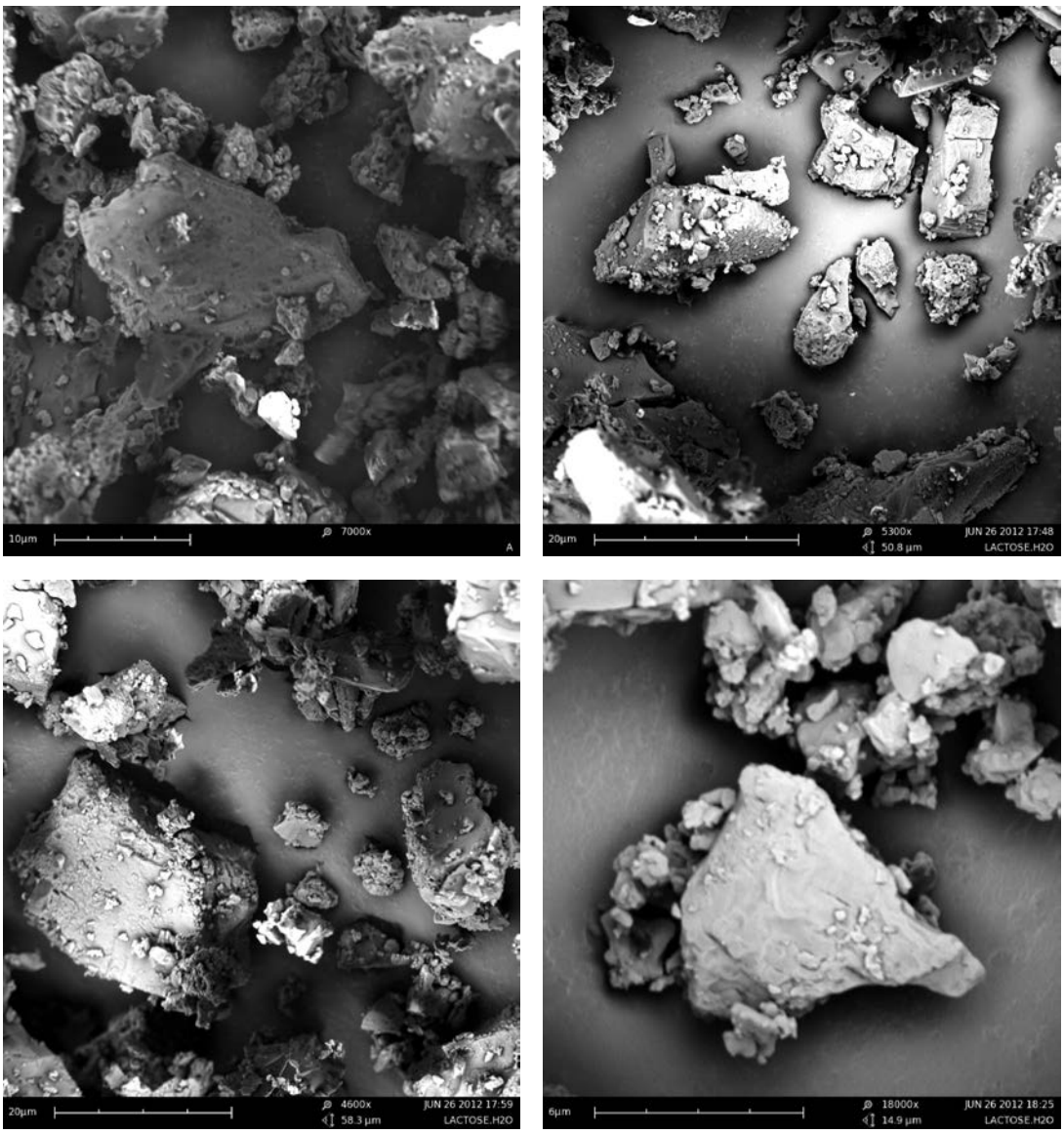

Figure 6: *SEM images of lactose powder particles. The shape of larger granules could be described as tomahawk-like as in Clydesdale et al. (1997) [33]. Small particles adhere to larger ones [8, 34]. Length scales were applied to assess heights of significant asperities.*

assumptions made. However, this approach might give another indication for appropriate asperity heights alongside SEM and AFM measurements. Eq. (8) was applied to SIA data of extreme size and convexity cases of lactose particles to establish a range of asperity heights. The results in **Table 5** show that the maximum of that range is estimated for a large particle with $d_{n,90}$ = 13.74 μm and a convexity $\omega_{n,10}$ to be about 0.8 μm. That range agrees reasonably with that derived from AFM measurements.

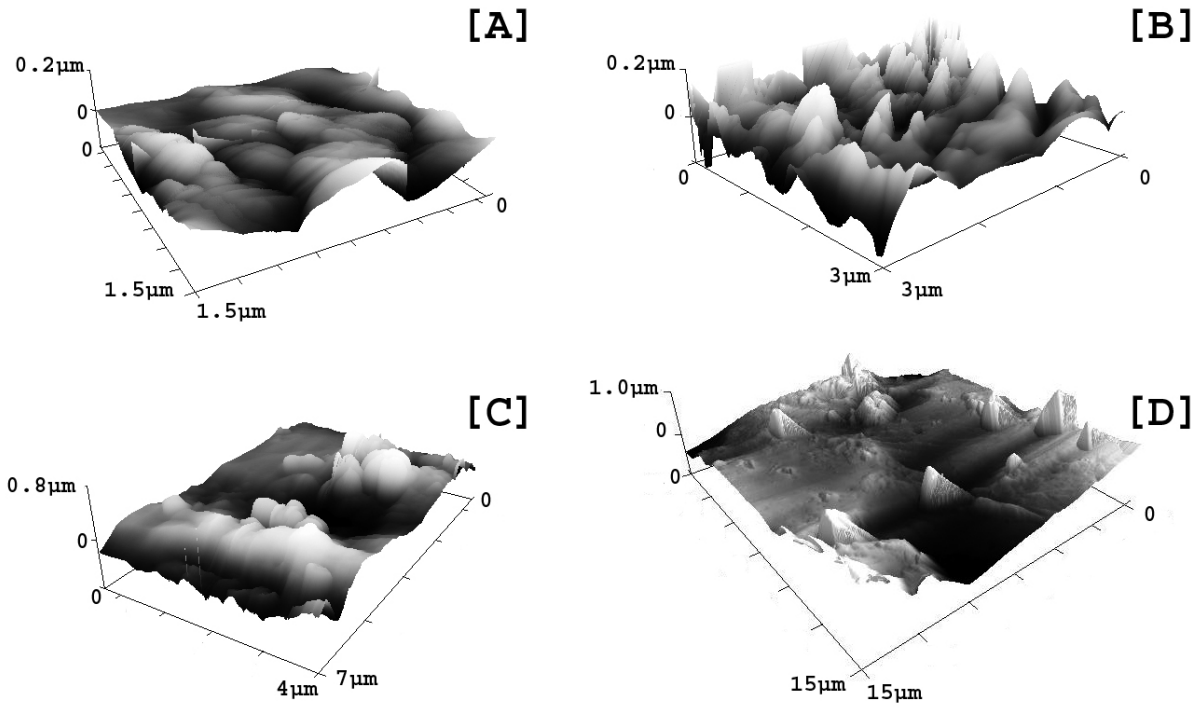

Figure 7: *AFM surface images of lactose powder particles for 2.25 µm² [A], 9 µm² [B], 28 µm² [C] and 225 µm² [D] surfaces of a lactose monohydrate powder sample.*

Table 5: *Roughness length scale h_a for lactose particles. Results obtained via Eq. (8) using quantile values of size and convexity data from SIA for small ($d_{n,10}$ = 1.42 µm) and large ($d_{n,90}$ = 13.74 µm), as well as smooth ($\omega_{n,90}$ = 0.99) and rough ($\omega_{n,10}$ = 0.90) particles. The range established agrees with the AFM results.*

h_a [µm]	$\omega_{n,10} = 0.90$	$\omega_{n,90} = 0.99$
$d_{n,10}$ = 1.42 µm	0.082	0.007
$d_{n,90}$ = 13.74 µm	0.796	0.071

4.1.4 Skeletal density

Pycnometry of 4 Granulac 230 lactose powder samples with Micromeritics AccuPyc 1330 pycnometer resulted in a skeletal (solid matrix) density of 1.561 ± 0.003 g/ml. This value is slightly higher than the literature value 1.545 g/ml for a different lactose powder product.

4.1.5 Porosity and crystallinity of lactose particles

An X-ray diffraction (XRD) analysis of one lactose powder sample resulted in the expected characteristic lactose monohydrate pattern. However, the comparison with a reference pattern revealed some differences. The average BET surface area of the lactose monohydrate powder samples was 0.85 $\pm$ 0.06 m^2/g. BET results were reproducible within 10% of the average. Takano et al. (2002) measured the BET surface area of lactose (Pharmatose 200M from DFE Pharma) with a primary particle diameter of $d_{v,50}$ = 27.1 μm and derived 0.56 m^2/g [7]. The BET surface area increased with decreasing particle size of milled lactose samples. The Granulac 230 lactose powder used in this study showed a slightly lower $d_{v,50}$ = 25 μm and thus fits that trend. Lactose particle porosity was calculated using 0.009 ml/g BET derived pore volume from BET measurement and the skeletal volume of 1.561 g/ml, resulting in 1% - 2% porosity which is at the low end of BET measurement applicability. A mercury intrusion measurement of lactose powder using 1800 psi as mercury filling pressure resulted in a porosity of 0.2%. Any present porosity in the lactose crystals may have been introduced by fractures during milling in the lactose manufacturing process. Milling is known to cause lactose to become partially amorphous [36]. The effect of possibly present initial particle porosity on granulation simulation has yet to be investigated to evaluate whether the initial particles can be assumed as non-porous and dry in computer models.

4.2 Granulation product (granules) characterisation

4.2.1 Particle size distribution and procedure reproducibility

Figure 8 presents the comparison between the results from granule sieving in this work (2012) and the results from an earlier work with the same granulation setup (2011) [20]. 95%-confidence intervals were computed using t-statistics in R. The average mean volumetric diameter $d_{v,\mathrm{mean}}$ of the granules is 2306 $\pm$ 214 μm. The highest mode $d_{v,\mathrm{mode}}$ lies consistently at 212 μm. The span_v is 12.0 for raw data and 11.6 for interpolated data. Concerning reproducibility of this granulation experiment, the graph shows some overlapping between the two distributions and similar trends. However, some size classes show distinct differences, e.g., classes 1 ($\leq$53 μm, fines) and 5 (150 - 212 μm), with possible sources of uncertainty affiliated with sieving equipment, such as coarse control of shaking intensity, sieve blocking and sample abrasion.

4.2.2 Surface and shape of lactose granules

Granules of selected size classes were imaged with SEM. **Figure 9** shows magnifications 15×, 50×, 100×, 500× and 2000× of the $\leq$75 μm, $\leq$300 μm, $\leq$850 μm and $\leq$4750 μm size classes. The shape of larger granules ($\leq$850 μm, $\leq$4750 μm) looks more spherical than for smaller granules which are rather irregularly shaped agglomerates ($\leq$300 μm) or even lactose particle-like tomahawks ($\leq$75 μm) [33]. Larger granules show larger pores between the agglomerated material of a granule than small granules. A comparison

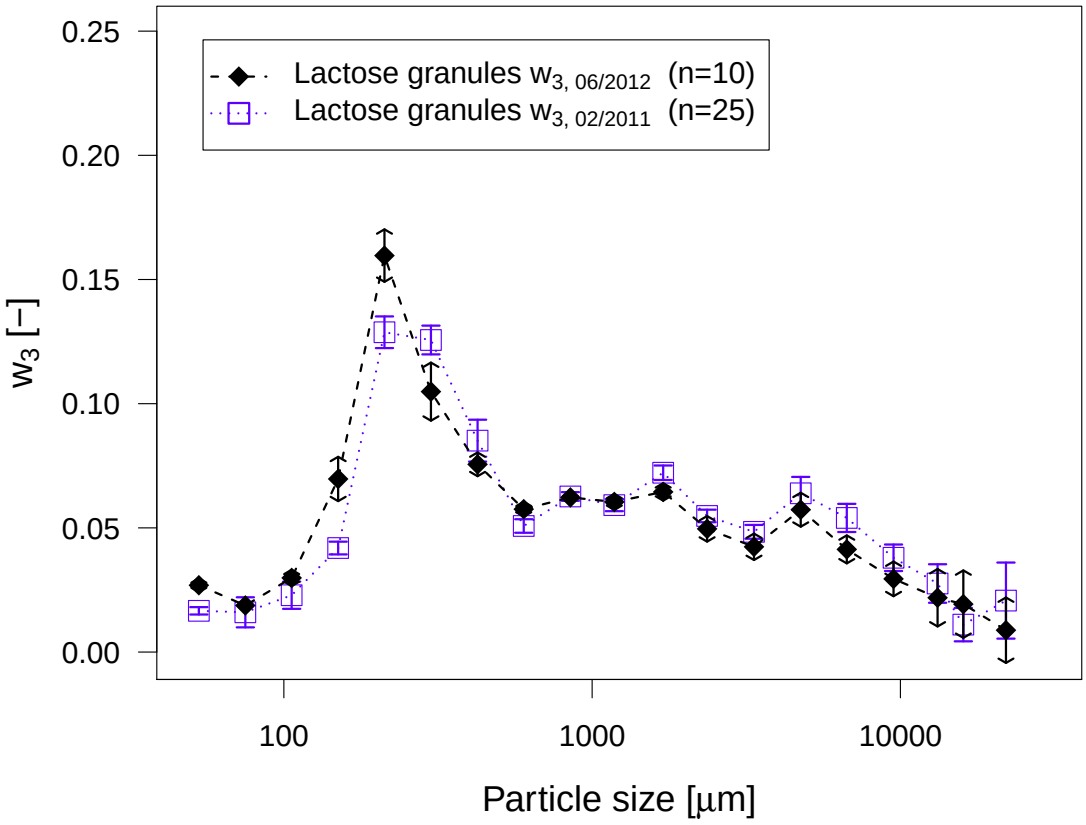

Figure 8: *Volume based particle size distribution (w_3) of the wet lactose granulation product granules. The results from 2011 [20] were reproducible with most obvious disparities in size classes 1 (fines $\leq$ 53 μm) and 5 (150 - 212 μm). Arrows and bars indicate 95% confidence intervals computed with t-statistic in R.*

between high magnification images of $\leq$75 μm and $\leq$4750 μm shows that the smaller material can be found in the large granule in agglomerated form, together with solidified bridges and fine particles.

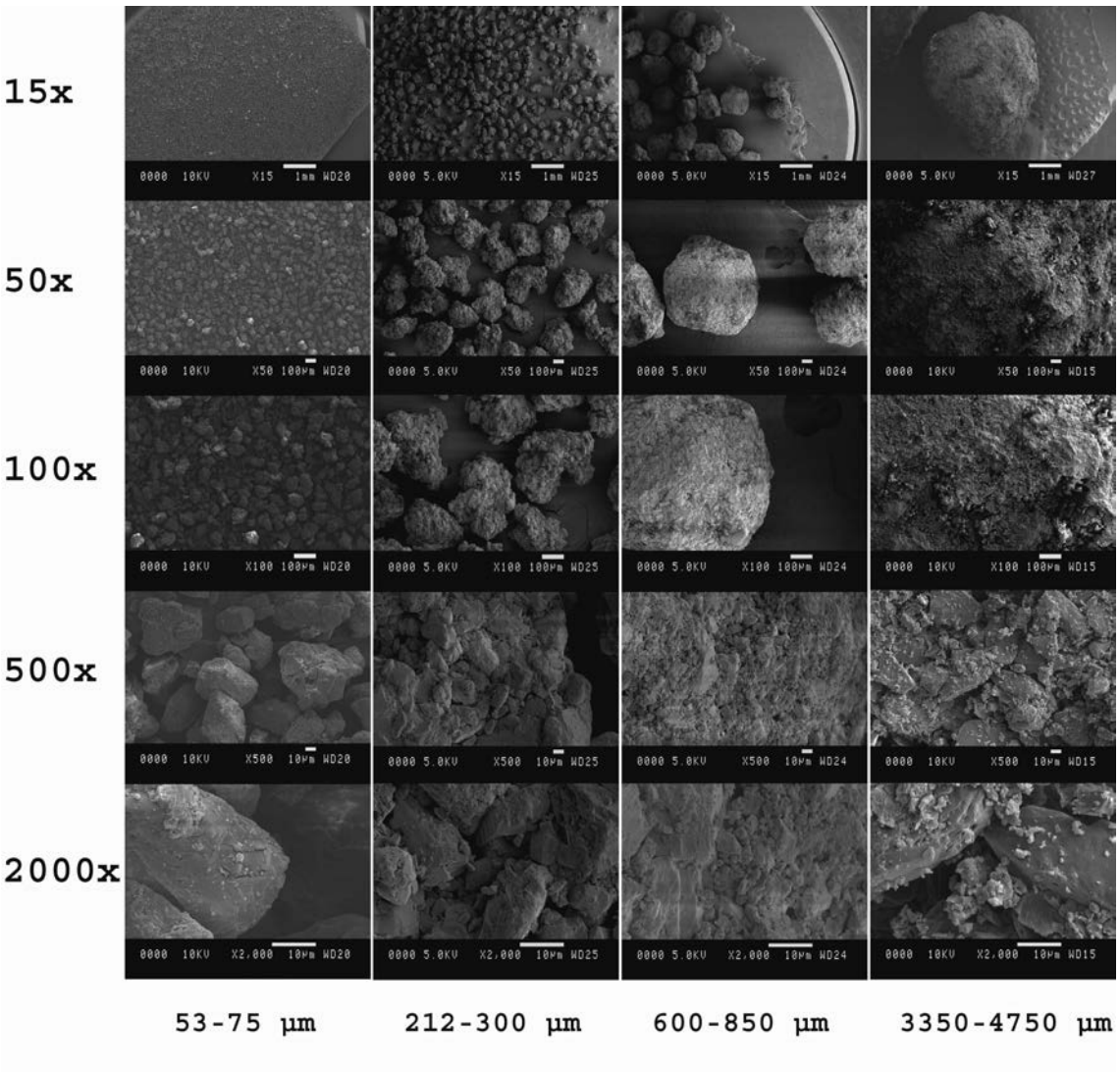

Figure 9: *SEM images of lactose granules. Larger granules exhibit are more spherical shape than tomahawk-like smaller particles [33]. Close-up images of larger granules look similar to the ones for small granules as those are possible constituents forming large granules.*

4.2.3 Porosity of lactose granules

μCT is limited in resolution and therefore was used to gain semi-quantitative and visual information about the granule porosity, and to compare with MIP. The MIP methodology is more robust and therefore was used for the appropriate quantification of granule porosity that shall be used later as a basis for computational modelling purposes. Figure 10 presents the μCT results of 'large-scale' ($\geq$ 4 - 14 μm pore size) porosity for the different size classes. A roughly log-linear upward trend is visible, indicating that larger granules show larger voids than smaller ones. In general, the voids formed from the agglomeration of larger particles are generally larger than the voids formed from the agglomeration of

smaller particles. Small size classes show less porosity which was expected due to the limited resolution of visible pores. Results for larger size classes show higher uncertainties due to small sample size. The loss of visual pore information is possibly more severe than the magnification factor can compensate for, which leads to deviations from the porosity trend in the lower size classes. The regression line was calculated based on measurements with more than 10 specimen (i.e. $\leq 4750\ \mu$m) to reach appropriate statistical significance. Linear regression (on the log-scale) of the data results in the line presented and clearly the confidence intervals often do not overlap with the line, which means that the relationship between large-scale porosity and size is probably more complex than log-linear.

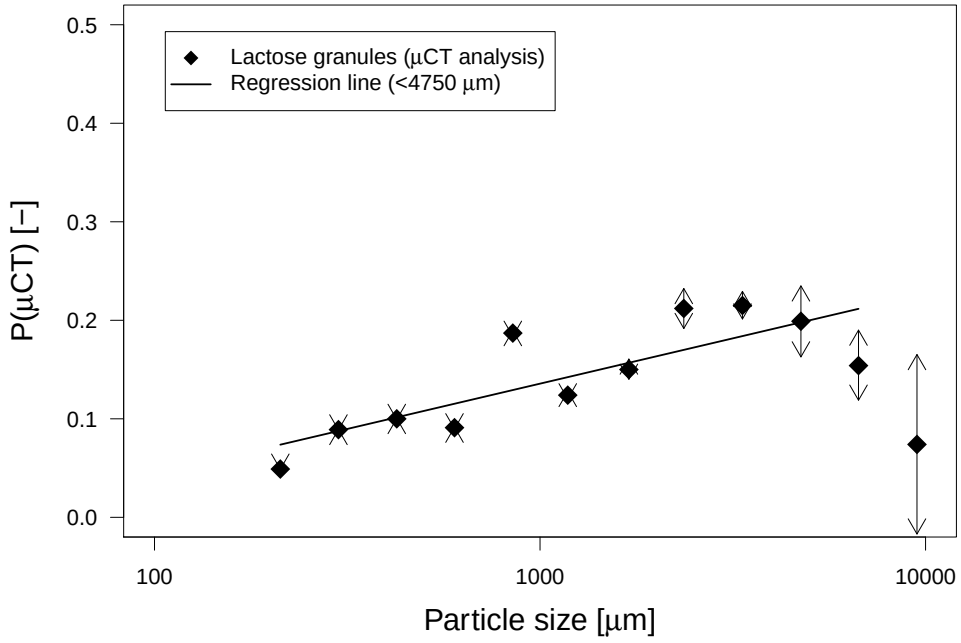

Figure 10: *X-ray tomography results for 'large-scale' porosity. The regression line was calculated based on measurements with more than 10 specimen (i.e. $\leq$ 4750 mm) only. Confidence intervals represent variance among particles in one measurement. Large particle measurement was limited to few particles, which lead to larger confidence intervals.*

Figure 3 shows that some granules exhibit heterogeneity in their internal structure, i.e. a very dense core, sometimes comprising large holes, and a more equally distributed porosity in the outer shell. Single granule measurement allows for the evaluation of porosity along one dimension of a granule. **Figure 11** tracks the void fraction along the height of an upper part of a $\leq$9500 μm granule. The part closer to the granule edge shows higher porosity than the denser core part. More granules would have to be investigated to draw a more solid conclusion.

Figure 12 and **Table 6** present the absolute porosity results derived from MIP and show the effect of insufficient filling pressure by comparing the adjusted to the non-adjusted results. The need for filling pressure correction is represented by the sudden increase in porosity in the size classes $\leq 600\ \mu$m. The general trend of corrected porosities shows an

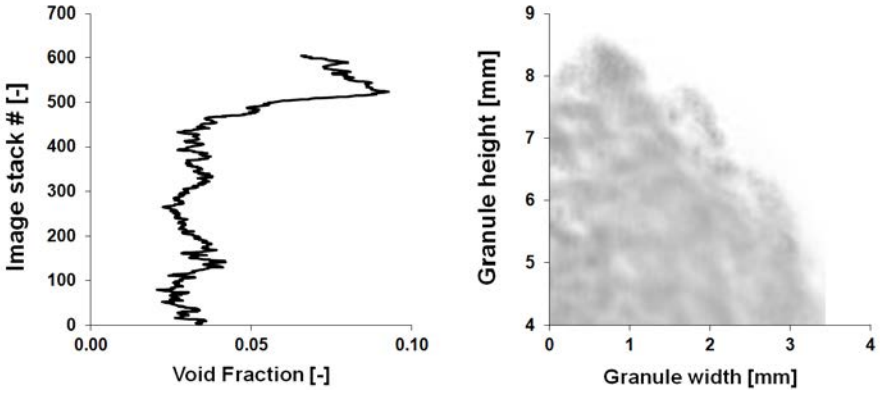

Figure 11: *Visualisation of porosity (void fraction) along the height of a single $\leq$ 9500 μm lactose granule. The left image shows the void fraction for each image along the image stack which corresponds to the particle profile on the right. The granule shows higher porosity in the outer shell part than in the core.*

increase in porosities along the size classes from about 30% to 40%. A similar trend was observed via X-ray tomography analysis as well, however, that accounted for 'large-scale' porosity only. Large voids connected to smaller pores were observed for larger granules in X-ray images (see Figure 3), similar to results by Farber et al. (2003) [31]. SEM images also suggest larger granules to have a more open structure, allowing for larger pores in general (compare 500$\times$ magnification images in Figure 9). Therefore, larger granules have a higher potential porosity due to increased maximum possible pore size. The results were compared to those reported by Mangwandi et al. (2010) who used the same material with similar process conditions. Their granules in the size class 1000 - 1180 μm showed a porosity of 26% which is lower than our result (35%). Possible reasons may be their increased impeller speed and extended granulation time, which were reported to have a reducing effect on granule porosity by Wikberg and Alderborn (1991) [10].

Deviations of the measurements from the trend, especially in the lower size classes, are probably affected by the assumptions made during recalculation of the filling pressures. The estimation of interstitial space becomes increasingly difficult with decreasing particle size because the assumption of spherical granules is less valid for small granules as observed in images from SEM (see Figure 9). Due to the irregular shape, interstitial space can be non-spherical and the minimum diameter can be much smaller. That may lead to underestimation of porosity. Further it has to be noted that the filling pressures required did not always exactly match the available data. Therefore, the value for cumulative mercury intrusion volume of the available pressure data point closest to the one required was used.

Farber et al. (2003) found MIP to give more accurate results while μCT provides detailed morphological information. The same observation was made in this study as mercury porosimetry was not limited in measurable pore sizes, if applied with the correct filling pressures, as much as μCT. However, μCT can provide useful visual information about the large-scale porosity structure.

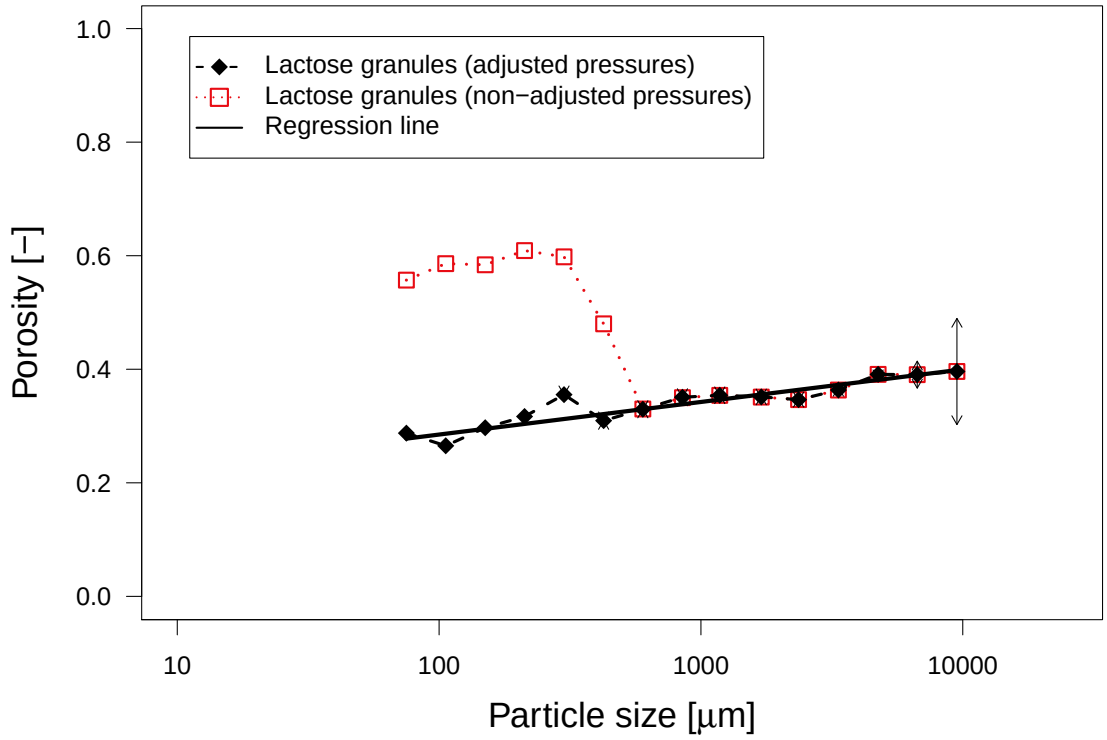

Figure 12: *Lactose granule porosity derived from mercury intrusion porosity. The non-adjusted porosity trend (red) shows the influence of inappropriate filling pressure, i.e. 1.02 psi for smaller size classes. Actual porosities (black) are calculated with filling pressures corrected via the Washburn equation. Confidence intervals were calculated based on 1% observed experimental standard deviation and the estimated sample size n.*

4.2.4 Single granule compression strength

Figure 13 presents the compression strength derived from single granule compression tests. The strength follows a negative log-linear trend with increasing granule size. The irregular shape and deformability of the granules as well as the admittedly small sample size lead to fairly large confidence intervals. The use of the highest peak for strength measurement can be considered reasonable in a chemical engineering background, e.g. during tabletting of a pharmaceutical tablet, when the highest compression strength of the granules is of interest [1]. However, such an approach may be inappropriate in dealing with biomedical materials where the very first and possibly partial failure of a medical implant is crucial.

The strength results were also compared to those reported by Mangwandi et al. (2010). They report 0.63 $\pm$ 0.02 MPa as the compression strength of granules in the 1000 - 1180 μm size class which is lower than the compression strength found in the same size class in this work (0.76 $\pm$ 0.17 MPa). As for particle porosity, the difference may be a consequence of different process conditions, e.g. 25% higher impeller speed and 1 min

Table 6: *Granule porosity calculated from MIP with filling pressure correction. n is the estimated number of particles per measurement, used for confidence interval calculations. ρ_e and ρ_s are the envelope and skeletal densities, calculated at adjusted mercury filling pressure and highest pressure, respectively. From those, particle porosity P for each size class was derived.*

Size [$\leq \mu m$]	n [-]	ρ_e [g/ml]	ρ_s [g/ml]	P [-]
	Mercury intrusion porosimetry			
75	895316	1.010	1.418	0.288
106	359187	1.004	1.366	0.265
150	118390	0.954	1.356	0.297
212	59018	0.943	1.381	0.317
300	22118	0.915	1.419	0.355
425	7868	0.995	1.441	0.310
600	3430	0.948	1.414	0.330
850	1773	0.976	1.503	0.351
1180	596	0.981	1.519	0.354
1700	152	0.957	1.476	0.351
2360	75	0.964	1.475	0.347
3350	20	0.910	1.419	0.358
4750	10	0.942	1.546	0.391
6700	4	0.946	1.551	0.391
9500	2	0.876	1.450	0.396

longer post-binder addition mixing, and strength measuring principles.

5 Conclusion

A multivariate data set for both the initial material, Granulac 230 α-lactose monohydrate powder, and the product granules of a high-shear wet granuluation process in individual size classes was established. It can be used as a data set for granulation modelling. The particles were characterised with respect to size, shape, porosity and strength using various analytical methods. The comparison with other works using similar materials and experiments showed agreements but also distinct differences. For example, the effect of sonication on sample preparation for laser scattering was surprisingly found to be minimal while the general particle size data showed agreements with the literature.

The use of several techniques per measured property allowed for the assessment of applicability and reproducibility of the methods. Important aspects identified for the characterisation methods used were:

- Porosity for small to large sizes of lactose granules can be readily quantified using mercury intrusion porosimetry (MIP) when a correction to the standard mercury

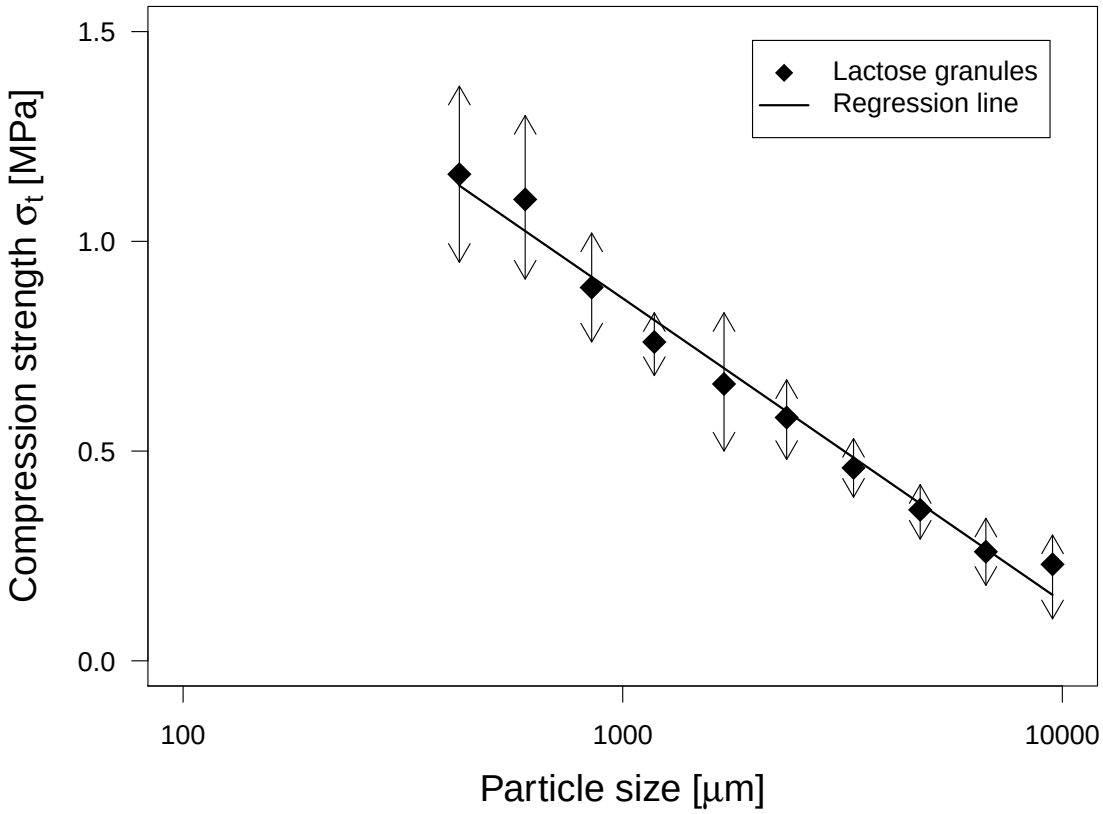

Figure 13: *Compression strength derived from single granule compression tests. At least 10 granules were tested for every size class. Compression strength was calculated from the highest observed peak at low strain, which was found to correspond to major granule failure indicated by a meridian crack along the granule [13].*

filling pressures is applied to account for filling of small interstitial spaces. Lactose granules showed absolute porosities increasing from 30% to 40% along the size classes. MIP results were reproducible within $\leq$ 1% for 3 size classes with 2 samples each. MIP can be aided by non-invasive X-ray tomography (μCT) as that gives useful visual information about pore structure. The resolution of the visual data is limited due to magnification and therefore quantitative analysis should be done with MIP. The statistical significance drops for both methods at large sizes (e.g. $\geq$ 6700 μm) as the sample space in a single measurement is limited.

- Surface roughness investigation of lactose powder and granules using atomic force microscopy (AFM) is difficult as the measurement is limited by roughness itself. The data derived from AFM is quantitatively precise but measurement fails on highly non-smooth surfaces. Granule parts can be mechanically affected by the cantilever. For fine particles the identification of single particles is difficult as visual resolution is limited. An AFM apparatus incorporating a scanning electron microscope (SEM) would be required to derive highly detailed surface characteris-

tics. Separate SEM measurements can provide high resolution images of particle surfaces but quantification of surface roughness is limited to visual 2D image scale. SIA derives shape information about particles and the convexity value can be used to estimate 2D surface roughness, as well. However, postprocessing methods for SIA have to be validated and need further investigation. The most useful results from surface investigation can be considered average values for heights of asperities from AFM to establish a range of possible roughness lengths, which agreed roughly with findings from SEM and SIA in this study.

- Strength measurements of granules are commonly performed using single granule compression testing. For fragmenting and semi-plastic deforming materials such as lactose granules the experimental data has to be processed carefully as the stress plots do not present unambiguous information about granule failure. Specifically, partial failure may be characterised by the first observed stress peak while the major part of a granule may fail with another but more significant peak along with a visible meridian crack. The irregular shape of lactose granules affects the contact area for compression stress which leads to increased variance in strength measurements. The compression strength of the granules, derived from the largest failure peaks at low displacement, followed a logarithmic decrease with size from 1.2 to 0.2 MPa.

In the future, the granulation experiment can be used to further study the impact of high-shear granulation mechanisms, for example binder viscosity, on the product. The presence and possible influence of dead zones in the mixer as not been studied yet and experimental techniques have to be developed to study such effects. Particle tracing simulations such as discrete element method (DEM) simulations that incorporate the actual granulator geometry can aid those investigations. DEM simulations also have the potential to quantitatively approach some of the rate constants that are currently estimated without experimental evidence [37, 38]. The mixing performance of the present granulator could be assessed using a tracer substance with the initial material. For pharmaceutical applications, a study involving the compression of the granules to sample tablets, possibly with a model active ingredient, would be desirable. The use of X-ray tomography offers more promising methods to evaluate the pore size distributions and shape characteristics.

6 Acknowledgements

The authors would like to thank the researchers at the Department of Chemical Engineering and the Department of Material Science for the cordial assistance and training on the analytical equipment, specifically Simon Griggs, Kendell Pawelec, Zlatko Saracevic, Wayne Skelton-Hough and Jin-Chong Tan. The financial support for Jan-Georg Rosenboom by the Solvay GmbH through the Ernest Solvay scholarship is gratefully acknowledged. Markus Kraft acknowledges support by the Singapore National Research Foundation under its Campus for Research Excellence And Technological Enterprise (CREATE) programme.

A Tables

Table A.1: *Particle size and shape distribution parameters (quantiles, mean and modes) derived from SIA measurements. ω is the particle convexity.*

Sample	$d_{n,10}$ [μm]	$d_{n,50}$ [μm]	$d_{n,90}$ [μm]	$d_{n,\text{mean}}$ [μm]	$d_{n,\text{mode}}$ [μm]
M1	1.31	4.38	14.39	6.81	3.86
M2	1.58	4.93	14.91	7.26	6.16
M3	1.28	3.58	11.44	5.49	3.21
M4	1.23	3.77	12.63	6.16	4.24
M5	1.42	4.63	14.55	6.83	5.11
M6	1.72	5.51	14.49	7.49	8.94
Average	1.42	4.47	13.74	6.67	5.25
Std. dev.	0.17	0.66	1.26	0.67	1.90
COV	12%	15%	9%	10%	36%

	$d_{v,10}$ [μm]	$d_{v,50}$ [μm]	$d_{v,90}$ [μm]	$d_{v,\text{mean}}$ [μm]	$d_{v,\text{mode}}$ [μm]
M1	14.68	40.64	74.33	43.40	52.63
M2	14.72	38.26	66.25	40.58	47.93
M3	11.97	37.09	75.57	40.41	63.41
M4	17.37	44.58	71.68	45.81	57.77
M5	13.21	34.36	70.68	38.21	57.77
M6	12.72	39.75	71.43	41.49	69.62
Average	14.11	39.11	71.66	41.65	58.19
Std. dev.	1.76	3.16	2.96	2.41	7.01
COV	12%	8%	4%	6%	12%

	$\omega_{n,10}$ [-]	$\omega_{n,50}$ [-]	$\omega_{n,90}$ [-]	$\omega_{n,\text{mean}}$ [-]
M1	0.88	0.96	0.98	0.94
M2	0.90	0.97	0.99	0.96
M3	0.91	0.98	1.00	0.97
M4	0.92	0.98	1.00	0.96
M5	0.90	0.97	0.99	0.96
M6	0.90	0.97	0.99	0.96
Average	0.90	0.97	0.99	0.96
Std. dev.	0.01	0.01	0.01	0.01
COV	1%	1%	1%	1%

Table A.2: *Particle size distribution parameters of lactose powder derived from laser scattering measurements. Each letter stands for a different sample and each number for a respective subsample. Sonication time (samples I and J) was 6 min.*

Sample	$d_{v,10}$ [μm]	$d_{v,50}$ [μm]	$d_{v,90}$ [μm]	$d_{v,\text{mean}}$ [μm]	$d_{v,\text{mode}}$ [μm]
			Non-sonicated samples		
E1	2.69	25.26	60.06	29.31	26.14
E2	1.70	21.57	58.05	27.16	19.76
E3	1.38	19.22	48.49	22.95	19.76
E4	1.48	20.01	51.13	23.82	21.69
G2	2.61	27.67	56.78	30.01	34.58
G3	1.84	27.76	56.85	29.67	34.58
G4	2.57	26.08	54.94	28.67	34.58
H1	3.71	31.08	61.03	33.09	37.96
H2	2.27	24.43	51.75	26.31	34.58
H3	2.04	22.75	46.73	24.38	26.14
Average	2.23	24.58	54.58	27.54	28.98
Std. dev.	0.66	3.56	4.61	3.04	6.67
COV	30%	14%	8%	11%	23%
			Sonicated samples		
I1	2.27	26.52	53.92	28.83	31.5
I2	2.08	24.40	51.06	26.24	31.5
I3	1.88	22.95	48.55	24.88	28.69
J1	2.70	27.77	54.57	29.63	31.5
J2	2.08	24.30	50.48	26.37	28.69
J3	2.29	24.06	49.73	25.93	28.69
Average	2.22	25.00	51.39	26.98	30.10
Std. dev.	0.26	1.63	2.17	1.68	1.41
COV	12%	7%	4%	6%	5%
			Samples combined		
Average	2.22	24.74	53.38	27.33	29.40
Std. Dev.	0.49	2.35	3.90	2.45	3.29
COV	22%	9%	7%	9%	11%

Table A.3: *Particle size distribution parameters of lactose powder derived from laser scattering using ethanol as the dispersant. Compared to the results using hexane, the average particle size characterisitics are higher and also the variance in the data is higher.*

Sample	$d_{v,10}$ [μm]	$d_{v,50}$ [μm]	$d_{v,90}$ [μm]	$d_{v,\text{mean}}$ [μm]	$d_{v,\text{mode}}$ [μm]
K1	4.87	28.84	56.26	30.19	37.96
K2	5.19	29.71	54.00	30.05	41.67
K3	9.27	38.63	70.62	39.80	45.75
M1	3.44	25.44	51.58	27.56	31.50
M2	4.82	27.30	52.11	28.41	34.58
M3	3.65	24.48	50.59	26.20	31.50
Average	5.21	29.07	55.86	30.37	37.16
Std. dev.	1.93	4.64	6.85	4.44	5.25
COV	37%	16%	12%	15%	14%

Table A.4: *Particle size distribution parameters of lactose granules derived from sieving analysis. Sample size was approximately 75 g each and sieving was performed for 20 min. The lower matrix reports the characteristic sizes using linear interpolation to derive the size at the actual percentile (e.g., $w_{3,i}$ = 10%) as opposed to the data in the upper matrix which is limited to the size class that falls below the percentile threshold (e.g., $w_{3,i} \leq 10\%$)*

Sample	$d_{v,10}$ [μm]	$d_{v,50}$ [μm]	$d_{v,90}$ [μm]	$d_{v,\text{mean}}$ [μm]	$d_{v,\text{mode}}$ [μm]
			Raw sieving data		
B101	106	300	4750	2125	212
B102	106	300	3350	1786	212
B103	106	425	3350	1902	212
B111	106	425	6700	2960	212
B112	106	425	4750	2608	212
B113	106	300	4750	2243	212
B114	106	300	4750	1921	212
B121	106	600	4750	2224	212
B122	106	425	4750	2410	212
B123	106	300	3350	2430	212
Average	106	380	4525	2261	212
Std. dev.	0	94	958	339	0
COV	0%	25%	21%	15%	0%

Table A.5: *Granule porosity per size class calculated from µCT image analysis. The table contains the void fractions (column 4) derived from the image stack analysis as outlined in Section 3. The correction factors for incomplete hole-filling and applied magnifications are presented in columns 5 and 6. Column 7 presents the corrected final values of 'large-scale' porosity ($\geq$ 4 - 14 µm pore size, due to limited resolution). n is the estimated number of specimen and Mag is the applied magnification.*

Size [$\leq \mu m$]	n [-]	Mag [-]	VF [-]	HFE [-]	MF [-]	$P_{\mu CT}$ [-]
	X-ray tomography analysis					
150	27778	70	0.016	2.7	0.71	0.032
212	9839	80	0.031	2.5	0.63	0.049
300	3472	70	0.048	2.6	0.71	0.089
425	1221	60	0.058	2.1	0.83	0.100
600	434	50	0.058	1.6	1.00	0.091
850	153	50	0.104	1.8	1.00	0.187
1180	57	50	0.085	1.5	1.00	0.124
1700	19	50	0.115	1.3	1.00	0.150
2360	16	40	0.142	1.2	1.25	0.212
3350	46	25	0.061	1.8	2.00	0.215
4750	17	20	0.066	1.2	2.50	0.199
6700	9	20	0.047	1.3	2.50	0.154
9500	3	20	0.030	1.0	2.50	0.074
13200	1	20	0.042	1.0	2.50	0.105

B Figures

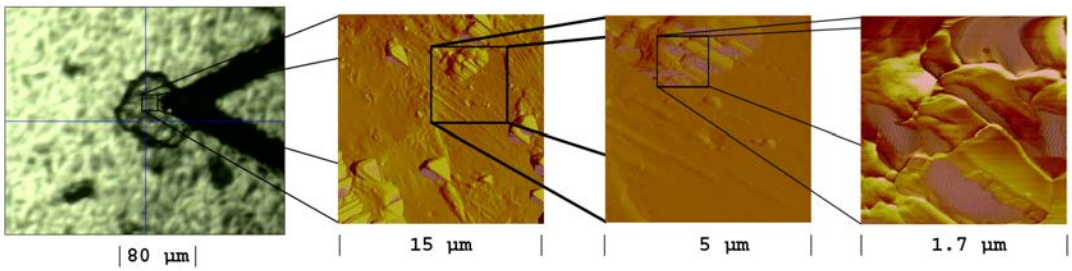

Figure B.1: *Particle surface approached by AFM tip during surface topography measurement. The left image shows the visual image from the tip camera that helps finding and focussing a spot to engage the tip to on the sample plate. The right three images show the resulting topography images of successful scanning with a tapping-mode tip on areas of different sizes around the same spot.*

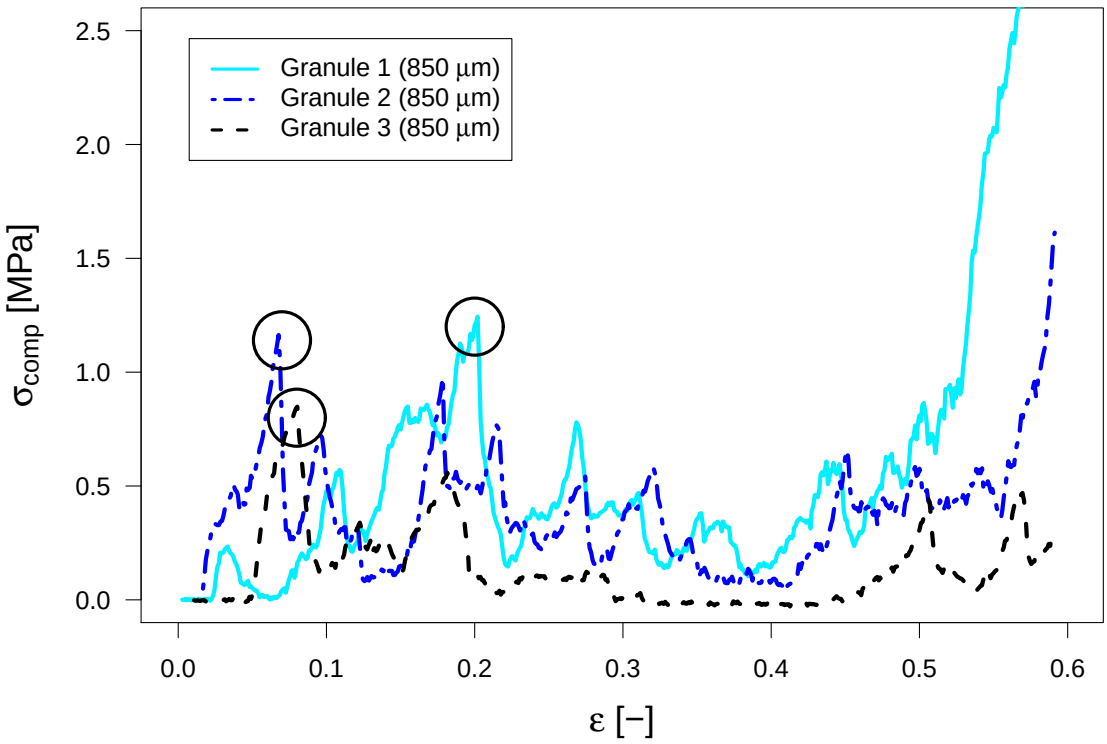

Figure B.2: *Compression strength test example plot for 600 - 850 µm granules. The material shows various peaks indicating partial failure of granule fragments. The highest peaks below ε = 0.4 were chosen for strength testing as they were found to correspond to the main granule failure indicated by a meridian crack [13]. Stress increase at larger displacements can be classified as compression of granule fragments and powder.*

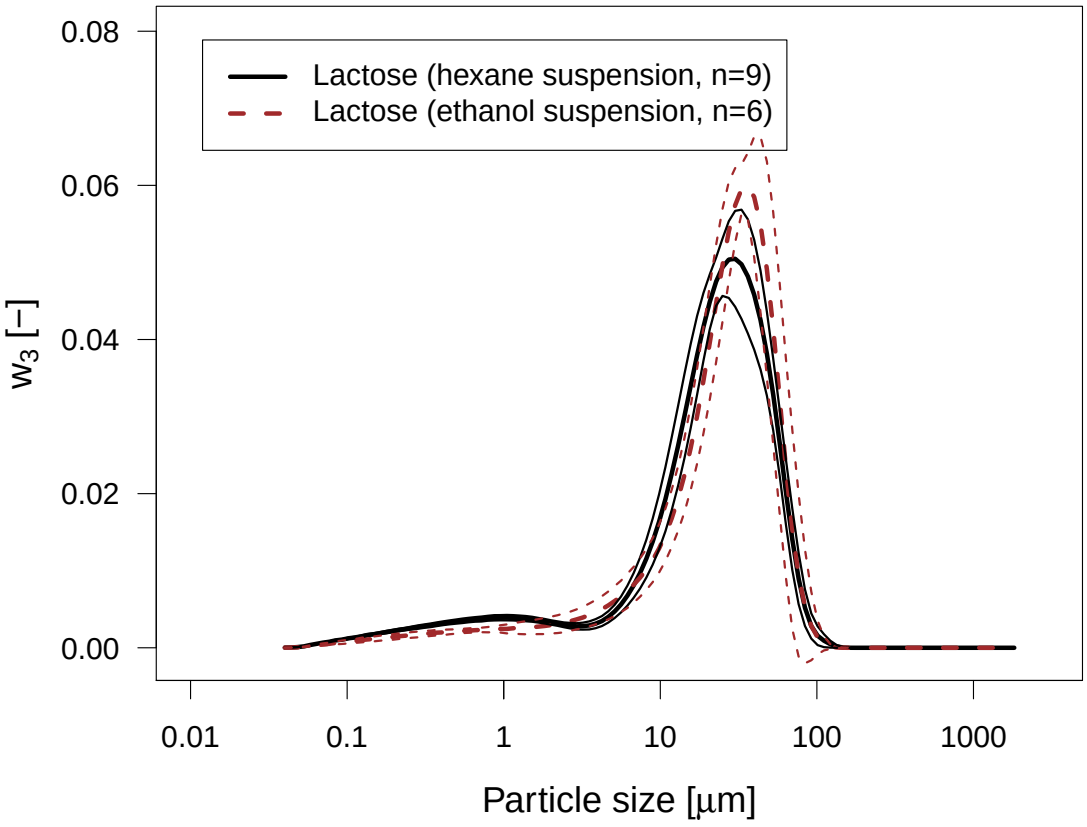

Figure B.3: *Volume based PSD for lactose monohydrate powder derived from non-sonicated laser scattering samples in hexane and ethanol suspension. The additional lines are 95% confidence bands. The PSD derived with ethanol is slightly shifted towards larger sizes and the separated fines peak is not clearly visible as for hexane based experiments.*

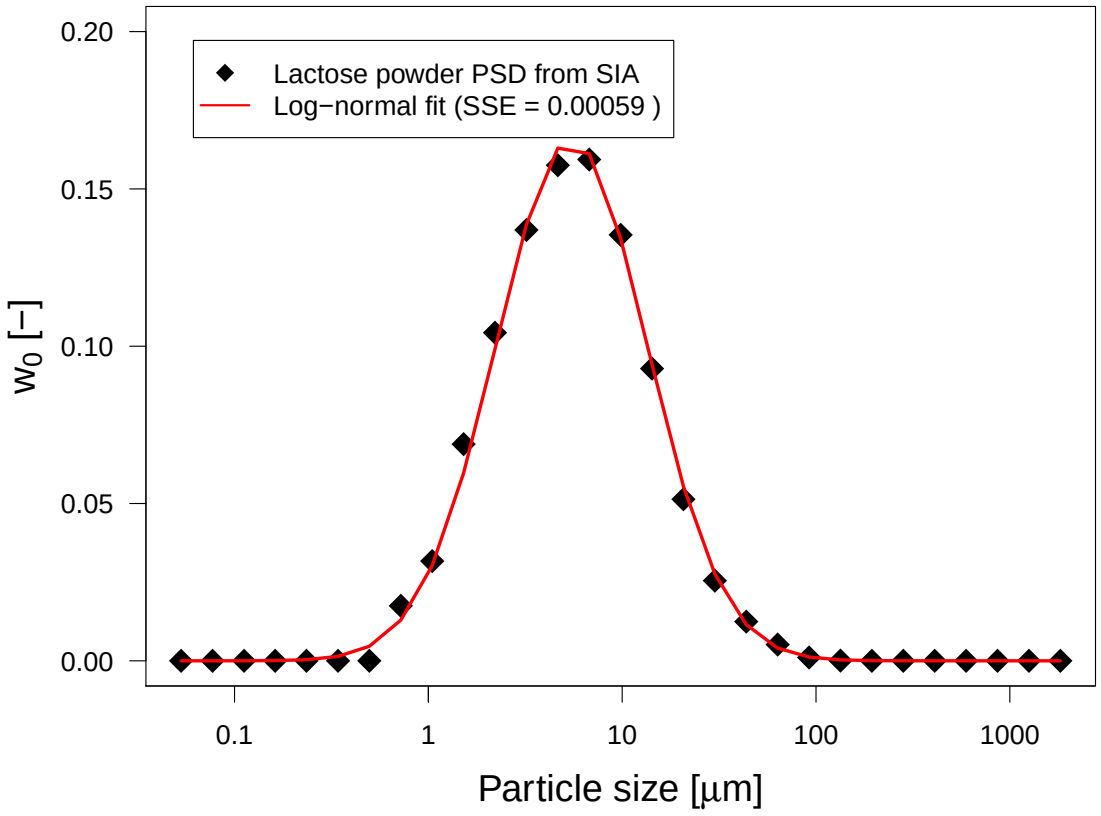

Figure B.4: *Lognormal distribution fit to SIA derived number based PSD. The describing lognormal location and shape parameters can be used for initial powder characterisation in granulation modelling [5]*

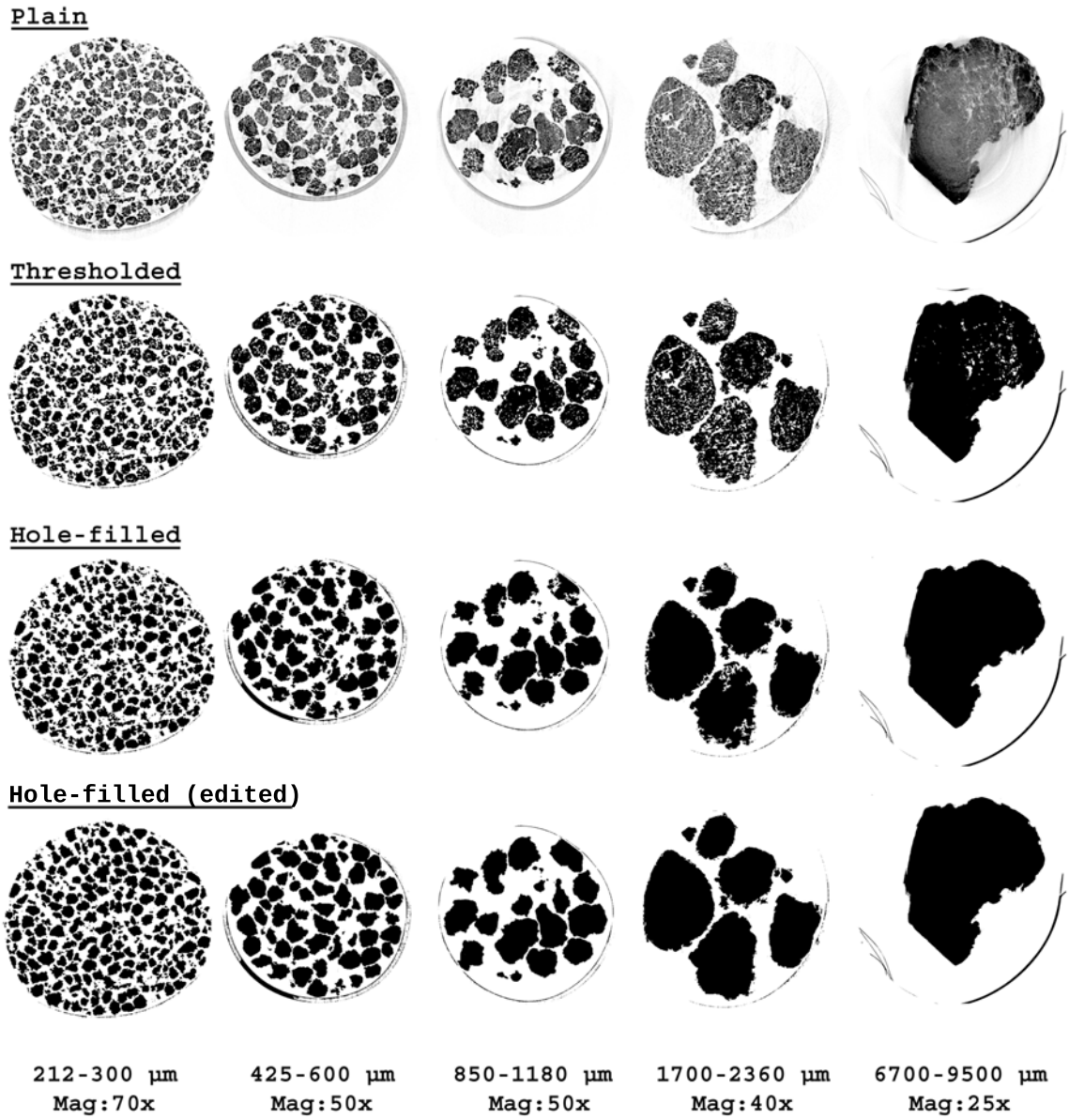

Figure B.5: *Examples for X-ray images of lactose granules in plain, thresholded, hole-filled and edited form for the visual analysis and quantification of granule porosity. Image processing was done using NRecon, ImageJ and PhotoShop.*

References

[1] Padma Narayan and Bruno C. Hancock. The relationship between the particle properties, mechanical behavior, and surface roughness of some pharmaceutical excipient compacts. *Materials Science and Engineering: A*, 355(1-2):24–36, 2003. ISSN 09215093. doi:10.1016/S0921-5093(03)00059-5.

[2] Robert H. Perry and Don W. Green. *Perry's chemical engineers' handbook*. McGraw-Hill, New York, 8 edition, 2008. ISBN 9780071422949.

[3] Michael M. Crowley, Britta Schroeder, Anke Fredersdorf, Sakae Obara, Mark Talarico, Shawn Kucera, and James W. McGinity. Physicochemical properties and mechanism of drug release from ethyl cellulose matrix tablets prepared by direct compression and hot-melt extrusion. *International Journal of Pharmaceutics*, 269 (2):509–522, 2004. ISSN 03785173. doi:10.1016/j.ijpharm.2003.09.037.

[4] Martin Rhodes. *Introduction to particle technology*. Wiley, Chichester, reprint. edition, 2001. ISBN 9780471984832.

[5] Andreas Braumann, Mike J. Goodson, Markus Kraft, and Paul R. Mort. Modelling and validation of granulation with heterogeneous binder dispersion and chemical reaction. *Chemical Engineering Science*, 62(17):4717–4728, 2007. ISSN 00092509. doi:10.1016/j.ces.2007.05.028.

[6] Simon M. Iveson. Limitations of one-dimensional population balance models of wet granulation processes. *Powder Technology*, 124(3):219–229, 2002. ISSN 00325910. doi:10.1016/S0032-5910(02)00026-8.

[7] Katsura Takano, Kazuo Nishii, Akiko Mukoyama, Yuki Iwadate, Hidehiro Kamiya, and Masayuki Horio. Binderless granulation of pharmaceutical lactose powders. *Powder Technology*, 122(2-3):212–221, 2002. ISSN 00325910. doi:10.1016/S0032-5910(01)00418-1.

[8] Handoko Adi, Ian Larson, and Peter Stewart. Laser diffraction particle sizing of cohesive lactose powders. *Powder Technology*, 179:90–94, 2007. ISSN 00325910. doi:10.1016/j.powtec.2007.01.018.

[9] C. Mangwandi, M.J Adams, M.J Hounslow, and A.D Salman. Effect of impeller speed on mechanical and dissolution properties of high-shear granules. *Chemical Engineering Journal*, 164(2-3):305–315, 2010. ISSN 13858947. doi:10.1016/j.cej.2010.05.039.

[10] Martin Wikberg and Göran Alderborn. Compression characteristics of granulated materials. iv. the effect of granule porosity on the fragmentation propensity and the compatibility of some granulations. *International Journal of Pharmaceutics*, 69(3): 239–253, 1991. ISSN 03785173. doi:10.1016/0378-5173(91)90366-V.

[11] Nejat Rahmanian, Ayman Naji, and Mojtaba Ghadiri. Effects of process parameters on granules properties produced in a high shear granulator. *Chemical Engineering Research and Design*, 89(5):512–518, 2011. ISSN 02638762. doi:10.1016/j.cherd.2010.10.021.

[12] Y. Hiramatsu and Y. Oka. Determination of the tensile strength of rock by a compression test of an irregular test piece. *International Journal of Rock Mechanics and Mining Sciences & Geomechanics Abstracts*, 3(2):89–90, 1966. ISSN 01489062. doi:10.1016/0148-9062(66)90002-7.

[13] Y.S Cheong, M.J Adams, A.F Routh, M.J Hounslow, and A.D Salman. The production of binderless granules and their mechanical characteristics. *Chemical Engineering Science*, 60(14):4045–4053, 2005. ISSN 00092509. doi:10.1016/j.ces.2005.02.033.

[14] H. Ryu and F. Saito. Single particle crushing of nonmetallic inorganic brittle materials. *Solid State Ionics*, 47(1-2):35–50, 1991. ISSN 01672738. doi:10.1016/0167-2738(91)90177-D.

[15] S. Antonyuk, S. Heinrich, J. Tomas, N.G. Deen, M.S. van Buijtenen, and J.A.M Kuipers. Energy absorption during compression and impact of dry elastic-plastic spherical granules. *Granular Matter*, 12(1):15–47, 2010. doi:10.1007/s10035-009-0161-3.

[16] Andreas Braumann, W. Wagner, and Markus Kraft. Numerical study of a stochastic particle algorithm solving a multidimensional population balance model for high shear granulation. *Journal of Computational Physics*, 229(20):7672–7691, 2010. doi:10.1016/j.jcp.2010.06.021.

[17] Andreas Braumann, Markus Kraft, and Paul R. Mort. Parameter estimation in a multidimensional granulation model. *Powder Technology*, 197(3):196–210, 2010. ISSN 0032-5910. doi:10.1016/j.powtec.2009.09.014.

[18] Andreas Braumann, Peter L. W. Man, and Markus Kraft. Statistical approximation of the inverse problem in multivariate population balance modeling. *Industrial & Engineering Chemistry Research*, 49(1):428–438, 2010. doi:10.1021/ie901230u.

[19] Andreas Braumann, Peter L. W. Man, and Markus Kraft. The inverse problem in granulation modelling – two different statistical approaches. *AIChE Journal*, 57 (11):3105–3121, 2011. doi:10.1002/aic.12526.

[20] Catharine A. Kastner, George Brownbridge, Sebastian Mosbach, and Markus Kraft. Impact of powder characteristics on a particle granulation model. *Chemical Engineering Science*, in press, 2013.

[21] J.R Jones and J. Bridgwater. A case study of particle mixing in a ploughshare mixer using positron emission particle tracking. *International Journal of Mineral Processing*, 53(1-2):29–38, 1998. ISSN 03017516. doi:10.1016/S0301-7516(97)00054-9.

[22] Alan Bleier. The roles of van der waals forces in determining the wetting and dispersion properties of silicon powder. *The Journal of Physical Chemistry*, 87(18): 3493–3500, 1983. ISSN 0022-3654. doi:10.1021/j100241a028.

[23] Inc Beckman Coulter. Coulter ls series product manual, 2011.

[24] Raymond C. Rowe, Paul J. Sheskey, and Marian E. Quinn. *Handbook of pharmaceutical excipients*. Pharmaceutical Press and American Pharmacists Association, London and and Chicago and Washington and DC, 6 edition, 2009. ISBN 0853697949.

[25] P. F. Fox and P. L. H. McSweeney. *Dairy chemistry and biochemistry*. Blackie Academic & Professional, London and and New York, 1 edition, 1998. ISBN 9780412720000.

[26] Pieter Walstra. *Dairy technology: Principles of milk properties and processes*. Marcel Dekker, New York, 1999. ISBN 082470228X.

[27] C. A. Beevers and H. N. Hansen. The structure of alpha-lactose monohydrate. *Acta Crystallographica Section B Structural Crystallography and Crystal Chemistry*, 27 (7):1323–1325, 1971. ISSN 05677408. doi:10.1107/S0567740871003947.

[28] Paul Webb and Clyde Orr. *Analytical methods in fine particle technology*. Micromeritics Instrument Corp., Norcross and Ga, 1997. ISBN 9780965678315.

[29] J. I. D'Souzae and More H. N. Mercury intrusion porosimetry : A tool for pharmaceutical particle characterization. *Pharmaceutical Reviews*, 6(2), 2008.

[30] E.W Washburn. Note on a method of determining the distribution of pore sizes in a porous material. *Proc Natl Acad Sci*, 7(4):115–116, 1921.

[31] Leon Farber, Gabriel Tardos, and James N. Michaels. Use of x-ray tomography to study the porosity and morphology of granules. *Powder Technology*, 132(1):57–63, 2003. ISSN 00325910. doi:10.1016/S0032-5910(03)00043-3.

[32] V. A. Folen. X-ray powder diffraction data for some drugs, excipients, and adulterants in illicit samples. *J Forensic Sci*, 20(2):348–372, 1975.

[33] Graham Clydesdale, Kevin J. Roberts, Gillian B. Telfer, and David J. W. Grant. Modeling the crystal morphology of alpha-lactose monohydrate. *Journal of Pharmaceutical Sciences*, 86(1):135–141, 1997. ISSN 0022-3549. doi:10.1021/js950496w.

[34] T.M Chitu, D. Oulahna, and M. Hemati. Rheology, granule growth and granule strength: Application to the wet granulation of lactose–mcc mixtures. *Powder Technology*, 208(2):441–453, 2011. ISSN 00325910. doi:10.1016/j.powtec.2010.08.041.

[35] J.A Greenwood and J.J Wu. Surface roughness and contact: An apology. *Meccanica*, 36(6):617–630, 2001. ISSN 00256455. doi:10.1023/A:1016340601964.

[36] Helen E. Newell, Graham Buckton, David A. Butler, Frank Thielmann, and Daryl R. Williams. The use of inverse phase gas chromatography to study the change of surface energy of amorphous lactose as a function of relative humidity and the processes of collapse and crystallisation. *International Journal of Pharmaceutics*, 217(1-2): 45–56, 2001. ISSN 03785173. doi:10.1016/S0378-5173(01)00589-0.

[37] S. Antonyuk, S. Heinrich, and I. Smirnova. Discrete element study of aerogel particle dynamics in a spouted bed apparatus. *Chemical Engineering & Technology*, 35 (8):1427–1434, 2012. doi:10.1002/ceat.201200083.

[38] L. Fries, S. Antonyuk, S. Heinrich, D. Dopfer, and S. Palzer. Collision dynamics in fluidized bed granulators: A dem-cfd study. *Chemical Engineering Science*, 86: 108–123, 2013.

Citation index